*J. Fluid Mech.* (2010), *vol.* 658, *pp.* 117–147.  
doi:10.1017/S0022112010001576

# Investigation of suction for laminar flow control of three-dimensional boundary layers

RALF MESSING AND MARKUS J. KLOKER†

Institut für Aerodynamik und Gasdynamik, Universität Stuttgart, Pfaffenwaldring 21, D-70550 Stuttgart, Germany

(Received 18 June 2009; revised 22 March 2010; accepted 27 March 2010; first published online 30 June 2010)

Direct numerical simulations are employed to investigate the effects of discrete suction orifices at the wall on the disturbance evolution in laminar three-dimensional boundary-layer flows with favourable pressure gradient. Suction panels with many suction orifices can excite unstable crossflow (CF) modes even if the orifice spacing is smaller than the chordwise/spanwise wavelengths of unstable modes, caused by imperfections in the orifice order or suction strength. It has been found that the most unstable steady vortex mode leads to strong CF vortices that invoke turbulence by secondary instability even on the active suction panel. The deliberate excitation and support of stabilizing vortices that have less than two-thirds of the spanwise wavelength of the most amplified ones – known from the upstream flow deformation or micrometre-sized roughness elements technique – by the orifice order on the panel can secure the desired stabilizing effect of suction and lower the necessary suction amount significantly.

**Key words:** control, drag reduction, stability

## 1. Introduction

For the next two decades a doubling of worldwide air traffic accompanied by a simultaneous shortage of crude-oil reserves is forecast. Therefore, it is highly desirable to reduce the fuel consumption of aircraft for environmental and economical reasons. As fuel consumption during cruise is mainly determined by viscous drag, its reduction offers the greatest potential for fuel savings.

One promising means to reduce viscous drag of a commercial aircraft is laminar flow control (LFC) by boundary-layer suction. Boundary-layer suction has been known for decades to delay laminar–turbulent transition by significantly enhancing the stability of the boundary-layer flow. For two-dimensional boundary layers the effect of suction is to make the wall-normal streamwise-velocity profile fuller by sucking a high-momentum fluid to the wall. For three-dimensional boundary layers it is the reduction of the crossflow (CF) that decreases the CF-related, dominantly inviscid instability that is typically strongest in the front part of a swept wing and leads to early laminar breakdown. In order to maintain laminar flow on a swept wing or a tailplane as far downstream as possible, it has been proposed to combine surface suction, applied in the leading-edge region, with extended regions of favourable pressure gradients, attained by profile shaping. This approach has been termed hybrid

† Email address for correspondence: kloker@iag.uni-stuttgart.de

LFC (HLFC). The goal of HLFC on swept surfaces of airliners is primarily to keep the regions of favourable pressure gradient laminar at cruise conditions. Suction in regions of adverse pressure gradient, including boundary-layer separation, is a different topic and is not discussed here.

Fundamental research to understand the underlying physical mechanisms, along with a plurality of flight experiments to address operational aspects, have been conducted, mainly in the USA and Europe. Outstanding overview articles by Joslin (1998*a*,*b*) summarize the numerous activities. The most important contributions are briefly mentioned in the following.

In the early 1960s the wings of the Northrop X-21 were equipped with spanwise suction slots nearly extending over the whole span, under the supervision of Werner Pfenninger, a suction pioneer. The wings had a sweep angle of 30°, and the suction slots were distributed over the full chord on both the top and bottom surfaces, each having a chordwise width between 75 and 250 μm, depending on their chordwise positions. The chordwise distance between successive slots varied between 2.5 and 5 cm. At suction rates $c_q = (0.5\text{–}1) \times 10^{-3}$, where $c_q$ is typically defined as the ratio of the spatially averaged suction velocity to the flight speed, laminar flow was maintained up to 96 % chord at global Reynolds numbers $Re \approx 20 \times 10^6$ in the outer part of the wing (Pfenninger 1965). Though successful, the suction-slot technique did not enter regular operation on airliners owing to enhanced maintenance and costs necessary to keep the slots clean. Owing to progress in manufacturing technologies enabling low-cost fabrication of microscale holes, perforated suction panels were used in the 1980s. Between 1985 and 1986 NASA performed flight tests on a Jetstar under various weather and flight conditions. On a 30°-swept wing a so-called glove was mounted to demonstrate the suitability of suction for daily use. The suction system consisted of 15 suction chambers that could be operated at different suction rates. The porosity of the glove surface was 0.25 %, the suction holes having a diameter of 65 μm and being regularly ordered at a distance of 890 μm. At a suction rate $c_q = 0.4 \times 10^{-3}$ averaged over all suction chambers, laminar flow along the entire glove was observed. Even a doubling of the suction rate did not cause premature transition to turbulent flow, a phenomenon otherwise often observed and termed oversuction. Moreover, it could be demonstrated that suction should be applied best in the vicinity of the stagnation point rather than too far downstream (Maddalon *et al.* 1989). Motivated by the promising results of the Jetstar flight-test campaign, a complete suction system based on the HLFC concept was developed for the wing of a Boeing 757. Flight tests at Mach numbers up to 0.82 and global Reynolds numbers $Re = 30 \times 10^6$ showed that laminar flow could be maintained up to 65 % chord. Unexpectedly, suction rates had to be only one-third of the values applied in the design process (Maddalon 1991).

In Europe intensive efforts aiming at an introduction of laminar-flow technology into civil aircraft construction did not set in until the mid-1980s. In France, Dassault Aviation conducted flight experiments with a Falcon 50 between 1987 and 1990. As in the Jetstar flight tests, attachment-line instability could be avoided by the use of a Gaster bump at the leading-edge root, preventing the attachment-line flow being contaminated by the turbulent fuselage boundary-layer flow. At small suction rates not affecting the total energy balance, the flow remained laminar up to 30 % chord at a sweep angle of 30° (Bulgubure & Arnal 1992). In 1987 Airbus Industries opted for the fin of an A320 as a test demonstrator to develop the HLFC technology for the operational readiness of a commercial aircraft (Thibert, Quast & Robert 1992). The fin was modified such that the perforated suction panels were integrated up to 20 % chord. In 1998 several flight tests were performed at Mach numbers around

0.8. Officially, the functionality of the system could be successfully demonstrated and laminar flow was detected up to 40 %–50 % chord, but a deeper evaluation of the obtained results is difficult for lack of detailed publications.

In order to get a deeper insight into the flow phenomena occurring in boundary layers with discrete suction through holes or slots, fundamental research has been carried out besides flight-test campaigns. Most of the work, both experimentally and numerically, has been done for two-dimensional boundary layers where no CF is present. The absence of any CF leads to fundamentally different boundary-layer flow physics compared to the inherently three-dimensional boundary layers on swept surfaces. Therefore, we point out that any direct transfer of findings gained from two-dimensional boundary layers to three-dimensional boundary layers is almost always misleading or even impossible. Recall that three-dimensional steady disturbance modes can be exponentially amplified eigenmodes only in three-dimensional boundary layers, whereas in two-dimensional flows, at most transient algebraic growth is possible, if growth can be observed at all. As an example, see the publication by MacManus & Eaton (1998). They addressed the possible problem of an interaction between suction-induced vortices and CF vortices in a three-dimensional boundary layer. Under the assumption that the formation of suction-induced longitudinal vortices in CF-dominated three-dimensional boundary layers is very similar to the process in two-dimensional boundary layers, they identified two length scales being relevant for nocent interaction and disturbance amplification. The first scale was the lateral distance between the vortices of a pair of vortices induced at each hole, and the second scale was the lateral distance between adjacent pairs of vortices of adjacent suction holes. Based on these considerations they derived a relationship indicating unfavourable ratios of spanwise hole spacing to hole diameter for a given boundary-layer thickness. As nocent interactions are likely to occur, these ratios should be avoided in design (see MacManus & Eaton 1998, figure 12). The fundamental flaw lies in the simplified assumption that knowledge transfer about vortex formation is feasible. In fact, in three-dimensional boundary layers only one longitudinal vortex is persistent downstream of each suction hole. Indeed, two counter-rotating vortices emanate from each suction hole, but as one vortex tries to induce a motion against the CF near the wall surface it is rapidly damped out (see figure 1). A further discussion of the basic research on two-dimensional boundary layers is outside the scope of this paper.

Because of their complexity, three-dimensional boundary layers have not been investigated often, either experimentally or theoretically. In France measurements were conducted at the F2-ONERA wind tunnel using a model wing with cylindrical leading edge at a sweep angle of 50°. The suction holes had a diameter of 45 μm and a distance of 1200 μm in the spanwise and chordwise directions. The major results of this measurement campaign were that initial disturbance amplitudes increased with increasing suction rates, but this negative effect was overcompensated by a reduced growth of the CF vortices, leading to a transition delay due to suction. By applying a suction rate $c_q = 1.8 \times 10^{-3}$ the initial amplitude rose by a factor of about 50 compared to the unsucked flow (Arnal, Seraudie & Archambaud 2000). At DLR Göttingen (Deutsches Zentrum für Luft- und Raumfahrt) the setup of the 'Prinzipexperiment Querströmungsinstabilität' (a basic experiment on CF instability; see Bippes 1999) was modified to enable investigations on the effects of suction in three-dimensional boundary layers (Abegg, Bippes & Bertolotti 1999; Abegg, Bippes & Janke 2000). At 16 % and 35 % chords of the flat plate two suction chambers were embedded that were covered by perforated metal sheets. Special attention was paid to the influence of the suction orifice geometry on disturbance

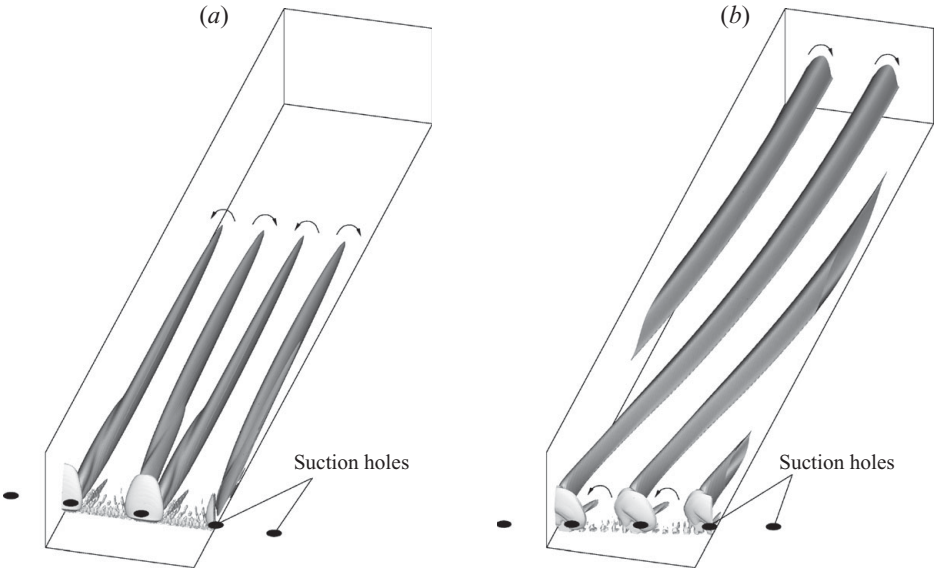


FIGURE 1. Visualization of vortical structures as gained from DNS of suction through a single spanwise row of holes on (*a*) an unswept plate and (*b*) a swept plate with favourable pressure gradient (sweep angle $\overline{\varphi}_\infty = 45°$). Arrows indicate sense of vortex rotation. Streamwise flow direction is from bottom to top. CF on the swept plate is from right to left. Note that in the case of the unswept base flow more suction has to be applied to get similarly strong vortices.

generation and amplification. Therefore, sheets with continuous spanwise suction slots, hereafter termed slits (chordwise slit width $\overline{d}_{SL} = 100\,\mu\text{m}$), and sheets with suction holes (hole diameter $\overline{d}_H = 50\,\mu\text{m}$ or $\overline{d}_H = 120\,\mu\text{m}$) were compared. Downstream of the second suction chamber, disturbance amplitudes of steady modes were measured for the various configurations. A comparison revealed that the slits generated the smallest disturbance amplitudes, followed by the large holes and the small holes. The increasing disturbance level was attributed to the increasing spanwise inhomogeneity of the suction distribution. Unsteady disturbances were damped by a factor of 20–30 when slits or large holes were applied, whereas no damping was noted with small holes compared to the no-suction case. As a possible explanation for this behaviour, Abegg *et al.* (2000) stated that the strong CF vortices could lead to an enhanced growth of low-frequency secondary disturbances. Finally, they concluded that excitation of three-dimensional disturbances has to be minimized by an appropriate suction distribution at the wall. A severe flaw of these experiments is, however, that flow similarity was not preserved. The perforated sheets used were originally designed for free-flight conditions. As the free-stream velocity in the wind-tunnel experiments was about one order of magnitude smaller than in free flight, similarity parameters, such as the ratio of hole diameter to displacement thickness $d/\delta_1$ and, in particular, the ratio of spanwise or chordwise hole spacing to displacement thickness $s_z/\delta_1$ or, respectively $s_x/\delta_1$, were not kept constant. Most importantly, the most unstable spanwise and chordwise wavelengths $\lambda_z$ and $\lambda_x$ are about one order of magnitude larger than that at flight conditions. Therefore, the hole spacings are unrealistically subcritical and the results have to be seen for an unrealistically 'ideal' quasi-homogeneous case.

Based on the spanwise homogeneous but streamwise varying suction, a number of studies were conducted to distribute the suction optimally with respect to objective functions; see e.g. Pralits, Hanifi & Henningson (2002) for an incompressible flow

and Pralits & Hanifi (2003) for a compressible flow. The optimal control theory based on the adjoint of the parabolized stability equations (PSE) and the boundary-layer equations is employed to find the optimal mean flow suction distribution in order to suppress the growth of convectively unstable disturbances. Pralits & Hanifi (2003) used as the control variable either the mass flow at the wall or the static pressure in pressure chambers below the wall, and as objective functions the kinetic energy of disturbances or the chordwise integral of the shape factor $H_{12}$. In the flow considered on the upper side of a commercial-aircraft wing, both small-amplitude CF and Tollmien–Schlichting disturbances could be significantly stabilized.

Direct numerical simulations (DNS) of discrete suction in three-dimensional boundary layers have only been published so far, to the authors' knowledge, by Bestek *et al.* (1996) and Spalart (1993). For suction through spanwise slits applied in an accelerated Falkner–Skan–Cooke (FSC) boundary layer, Bestek *et al.* compared results of their DNS with boundary-layer calculations using suction modelling. As the suction rates were low and upstream influence of suction was negligible, good agreement was achieved. Although only weak suction was applied, boundary-layer parameters such as the shape factor $H_{12}$ considerably altered over the suction slit and only slowly approached the values of the undisturbed flow downstream of the suction. Spalart performed DNS of suction through holes in the swept Hiemenz flow. For a single row of holes oriented in the spanwise direction, he showed that the receptivity of steady CF modes has its maximum near branch I of the instability chart. At first, the amplitudes of the steady disturbance modes transiently decay downstream of the hole row, regardless of the hole-row location within the instability domain. Only after some streamwise distance, depending on the location of the hole row, amplification of the CF modes sets in. For a hole array with many spanwise hole rows, observations were quite similar. Downstream of the first hole row the disturbance amplitudes decay until the vicinity of the second hole row, where the amplitudes are again lifted up, and so on. Hence, the disturbance amplitudes oscillate at the beginning of the array, and again disturbance growth sets in only after some streamwise distance. Spalart also performed simulations at strong suction rates, but, unexpectedly, did not observe oversuction. He explained this behaviour with the use of a smooth and steady suction distribution, the assumption of spanwise periodicity or the absence of any time-dependent forcing.

Recently, Bertolotti (2003) proposed an optimization algorithm, yielding a sophisticated suction orifice pattern that minimizes the excitation amplitudes of the suction pattern at amplified eigenvalue pairs of the stream- and spanwise wavenumbers. An advanced approach is necessary as the flow angle and the dispersion relation (of amplified disturbances) vary significantly downstream in a swept-wing boundary layer. Simple strategies successfully applied in two-dimensional boundary layers, such as anti-phased excitation through staggered hole orders to cancel upstream-induced disturbances, fail. However, the algorithm assumes small perturbations that do not alter the receptivity and dispersion properties of the base flow. For values of $c_q = v_{av}/U_\infty < 10^{-4}$, where $v_{av}$ is the spatially averaged suction velocity, this assumption is justified. In order to stabilize the boundary layer, higher suction rates have to be applied. In this case the resulting mean flow distortion is inherently not negligible and leads to a failure of the first-step optimization. Thus, an advanced optimization strategy must be elaborated, accounting for the mean flow alteration and the modified receptivity for a pattern supposed to work successfully at $c_q > 10^{-4}$. However, this is difficult when using only the PSE, as our simultaneous DNS investigations in cooperation with F. Bertolotti have shown. Moreover, only suction-induced disturbances are minimized with this strategy.

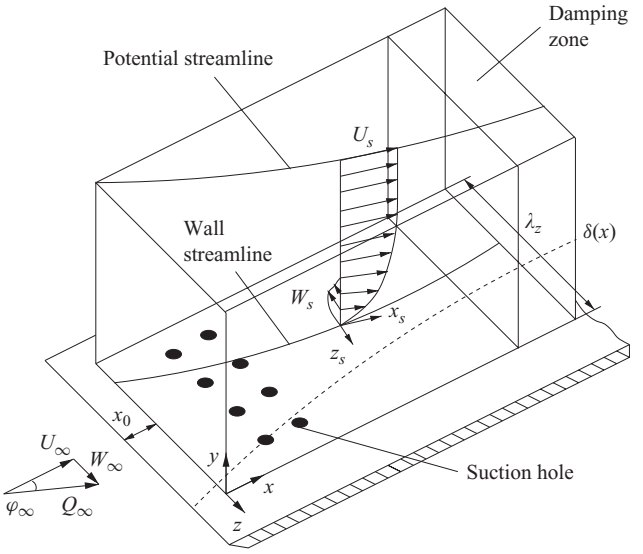


FIGURE 2. Integration domain and coordinate systems.

In this paper we investigate the physics of discrete suction in favourable-pressure-gradient boundary layers with CF by DNS, exploiting our previous studies on CF instability (see Wassermann & Kloker 2002, 2003, 2005; Bonfigli & Kloker 2007). Finally, 'formative' suction, the combination of the upstream flow deformation (UFD) technique (see Wassermann & Kloker 2002) with discrete suction, is demonstrated (see also Kloker 2008): the suction orifices are ordered such that they generate CF vortices with narrow spanwise spacing that do not cause secondary instability and suppress the dangerous most unstable steady modes. This paper is organized as follows: § 2 presents the numerical method and its verification with DNS results by Spalart (1993), and § 3 the underlying base flows for the investigations of suction. In § 4 the fundamental relationship between discrete suction and generation of unstable disturbances is discussed. In § 5 the results of conventional suction are discussed, and § 6 provides an example of formative suction.

## 2. Numerical method

### 2.1. *Governing equations and discretization*

The numerical method solves the three-dimensional, incompressible and unsteady Navier–Stokes equations in vorticity–velocity formulation. All variables are normalized by the reference length $\bar{L}$ and the chordwise reference velocity $\bar{U}_\infty$. The global reference Reynolds number is $Re = \bar{U}_\infty \bar{L}/\bar{\nu}$, where the overbar denotes dimensional variables and $\bar{\nu}$ is the kinematic viscosity. The equations are solved in a rectangular integration domain with a Cartesian grid on a flat plate fixed at a distance $x_0$ from the leading edge. The chordwise direction is denoted by $x$, the wall-normal direction by $y$ and the spanwise direction by $z$ (see figure 2). The corresponding velocity and vorticity vectors are $\boldsymbol{u} = \{u, v, w\}^T$ and $\boldsymbol{\omega} = \{\omega_x, \omega_y, \omega_z\}^T$.

The solution of the Navier–Stokes equations is carried out in two successive substeps. At first, a steady laminar base flow (index $B$) is calculated satisfying the assumptions of a spanwise infinite swept plate ($\partial/\partial z = 0$, but $w_B$, $\omega_{xB}$, $\omega_{yB} \neq 0$). The chordwise acceleration of the potential flow induces a CF component in the

boundary layer. In the second step arbitrary steady and/or unsteady disturbances are introduced in this laminar base flow and the disturbance flow, denoted by a prime, is calculated.

Assuming periodicity at the lateral boundaries we use a complex Fourier spectral representation to calculate the non-symmetric three-dimensional disturbance flow:

$$f'(x,y,z,t) = \sum_{k=-kmax}^{kmax} \hat{f}_k(x,y,t)\,\mathrm{e}^{\mathrm{i}k\gamma_0 z}, \qquad \mathrm{i}=\sqrt{-1}, \qquad \hat{f}_k \in \mathbb{C}. \tag{2.1}$$

At the wall, $y=0$, the no-slip condition is satisfied for $u'$ and $w'$. Suction at the wall is modelled by prescribing a steady wall-normal velocity distribution

$$v'(x,0,z) = -v_c \cos^3\left(\frac{\pi r}{d}\right), \tag{2.2}$$

within the perforations. This function runs out smoothly at the perforation ends with zero, first and second derivatives, and eases comparison with the work of Meitz & Fasel (1995) for two-dimensional base flows. For finite spanwise suction slots with a slot width $d_{SL}$, the extension in the chordwise direction, and a slot length $L_{SL}$, the extension in the spanwise direction, or circular suction holes with a diameter $d_H$, the following hold.

Suction slot: for $z_{SL} \leqslant z \leqslant z_{SL}+L_{SL}$, i.e. in the core region of the slot,

$$d = d_{SL}, \quad r = \sqrt{(x-x_{SL})^2}, \quad r \leqslant \frac{d_{SL}}{2}; \tag{2.3}$$

for $z < z_{SL}$, at the left end of the slot,

$$d = d_{SL}, \quad r = \sqrt{(x-x_{SL})^2+(z-z_{SL})^2}, \quad r \leqslant \frac{d_{SL}}{2}; \tag{2.4}$$

for $z > z_{SL}+L_{SL}$, at the right end of the slot,

$$d = d_{SL}, \quad r = \sqrt{(x-x_{SL})^2+(z-(z_{SL}+L_{SL}))^2}, \quad r \leqslant \frac{d_{SL}}{2}. \tag{2.5}$$

Suction hole:

$$d = d_H, \quad r = \sqrt{(x-x_H)^2+(z-z_H)^2}, \quad r \leqslant \frac{d_H}{2}. \tag{2.6}$$

The centreline of the suction slot and the centre of the suction hole are located at $(x_{SL},0)$ and $(x_H,0,z_H)$, respectively. At the lateral ends of the slots at $(x_{SL},0,z_{SL})$ and $(x_{SL},0,z_{SL}+L_{SL})$, a smooth changeover to vanishing suction is prescribed by adding the suction distribution of a semi-hole. The maximum suction velocity at the centreline of the slot or at the centre of the hole is given by $v_c$. Perspective views of the suction-velocity distributions over a slot and a row of holes are shown in figure 3. The average suction velocity over a hole is $0.218v_c$, and over the core region of a slot, it is $0.424v_c$. Keeping $v=v_c$ constant, i.e. using a top-hat profile, the effective hole diameter is then $0.467d_H$, or the slot width is $0.424d_{SL}$.

Besides suction, defined steady and unsteady disturbances with a spanwise wavenumber $k\gamma_0$, frequency $h\omega_0$, forcing amplitude $A_{h,k}$ and phase $\Theta_{h,k}$ can additionally be introduced into the laminar flow field at several disturbance strips. By using localized blowing and suction the disturbances are enforced with momentum

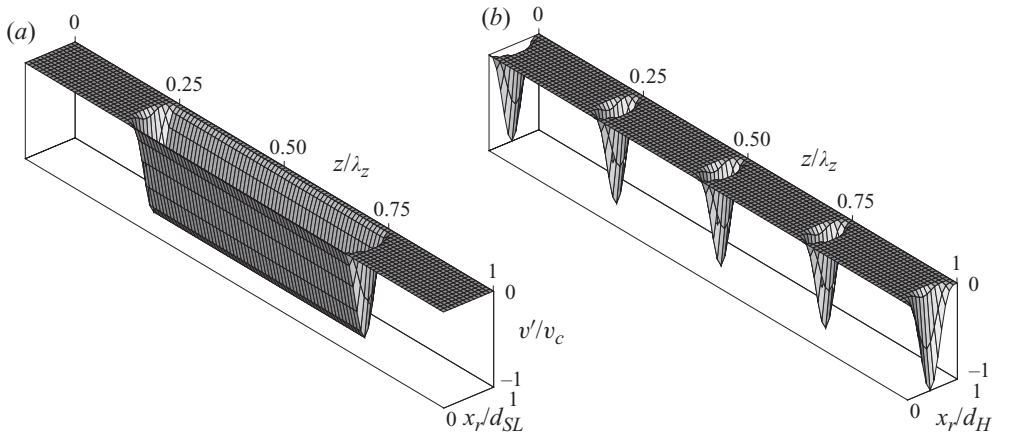


FIGURE 3. Spatial distribution of non-dimensionalized disturbance velocity $v'/v_c$ at the wall over one fundamental spanwise wavelength $\lambda_z$ at suction through (*a*) a spanwise slot with $L_{SL} = 0.5\lambda_z$ and (*b*) spanwise regularly ordered holes with $d_H \approx 1/20\lambda_z$. Note that the streamwise direction is stretched by a factor of 2.2 with respect to the spanwise direction; $x_r = x - (x_{SL} - (d_{SL}/2))$.

input but no net mass flow:

$$v'(x, y, z, t) = f_v(x) \left( \sum_{k=1}^{K} 2A_{0,k} \cos(k\gamma_0 z + \Theta_{0,k}) + \sum_{h=1}^{H} \sum_{k=-K}^{K} 2A_{h,k} \cos(k\gamma_0 z - h\omega_0 t + \Theta_{h,k}) \right), \quad (2.7)$$

where $f_v(x)$ is a piecewise defined symmetric fourth-order parabola with zero values, and zero first and second $x$-derivatives at the ends of the respective strip and a maximum value of 1; see Wassermann & Kloker (2002).

At the upper boundary of the integration domain $y = y_M$, the disturbance vorticity vanishes:

$$\hat{\omega}_{x,k}(x, y_M, t) = 0, \quad \hat{\omega}_{y,k}(x, y_M, t) = 0, \quad \hat{\omega}_{z,k}(x, y_M, t) = 0. \quad (2.8)$$

According to linear stability theory, exponential decay is prescribed for the wall-normal disturbance velocity

$$\frac{\partial \hat{v}_k(x, y_M, t)}{\partial y} = -\frac{\alpha^*}{\sqrt{Re}} \hat{v}_k(x, y_M, t). \quad (2.9)$$

Since suction is applied in the disturbance flow this assumption is not justified for the two-dimensional disturbance. In order to properly include the case of homogeneous suction with constant $v$-profile over $y$, the following distinction has been applied for the decay factor $\alpha^*$:

$$\alpha^* = 0, \quad \text{for} \quad k = 0,$$
$$\alpha^* = \sqrt{\alpha_r^2 + (k\gamma_0)^2}, \quad \text{for} \quad k > 0.$$

Compared to previously used and published versions of the numerical code, the multigrid method (see Wassermann & Kloker 2002) for solving the Poisson equation for the wall-normal velocity component $v'$ has been replaced by a direct

method. Thereby the flow variables of the discretized linear system of equations are transformed into Fourier space, yielding a decoupled system of ordinary differential equations in $y$, which in turn can be solved directly and independently (for details, see Swarztrauber 1977 and Messing, Kloker & Wagner 1998). This solution algorithm is quite effective, especially on shared-memory supercomputers. When compared to iterative line successive overrelaxation (LSOR) methods and a multigrid algorithm (with 5–6 V cycles) this direct method turned out to perform approximately twice as fast on the NEC-SX supercomputer series. Naturally, this specification can only serve as a rule of thumb, as various parameters such as the grid resolution influence the performance gain. More details on the complete numerical method are reported in Bonfigli & Kloker (1999) and Wassermann & Kloker (2002).

### 2.2. *Code verification*

First, a case for asymptotic suction on a flat plate has been computed, leading to a constant streamwise velocity profile for a zero-pressure-gradient boundary layer. Using the zero-wall-normal-slope boundary condition for $v$ at the upper boundary ($\alpha^* = 0$), a perfect agreement with the theoretical profile at $c_q = 0.5 \times 10^{-3}$ has been achieved (see Messing 2004). The only investigations suitable for a quantitative comparison of discrete suction are numerical simulations by Spalart (1993). He considered the swept Hiemenz flow at a Reynolds number $\overline{Re} = W_\infty/\sqrt{S\nu} = 400$, with $W_\infty$ being the spanwise velocity component and $S = \partial U/\partial x$ the strain rate in the chordwise direction. Suction through holes was modelled by a wall-normal velocity distribution with Gaussian-type shape at the wall. Two cases have been chosen for comparison, namely a single row of holes with a spanwise hole spacing $\lambda_z = 10$ and the radius of the Gaussian $\sigma = 2$, and an array of suction holes with a chordwise hole spacing $\lambda_x = \lambda_z$ and again $\sigma = 2$. The average suction rate is $v_0 = 10^{-6} W_\infty$, yielding a peak suction rate at the hole centre of $7.96 \times 10^{-6} W_\infty$. Note that all lengths are normalized with the attachment-line thickness $\delta_l = \sqrt{\nu/S}$. In accordance with Spalart's approach, the Gaussian-type suction distribution was implemented in our numerical method to perform code verification. In order to compare the results, the maximum of $u'$ over $y$, $u'$ representing the r.m.s. value of the chordwise component $u$ with respect to its $z$-average, is computed and normalized by $v_0$. In our simulations the chordwise step size is $\Delta x = 0.5$ for the single-hole-row case and $\Delta x = 0.25$ for the hole array. In the wall-normal direction a stretched grid has been used with the smallest wall-normal step size $\Delta y = 0.013$ at the wall. We used this fine grid resolution to secure a grid-independent solution. Results are shown in figure 4. For both cases excellent agreement is achieved, as not only growth rates but also the quite complicated receptivity mechanisms match.

## 3. Laminar base flows

Two different laminar base flows are used for the following investigations. In order to examine the more fundamental effects of discrete suction in three-dimensional boundary-layer flows, an accelerated FSC boundary layer on a swept wedge has been chosen. The advantage of such an approach is that the flow is well defined by the Hartree parameter $\beta_H$ and the sweep angle $\overline{\varphi}_e$. For boundary-layer flows, as they occur on operating commercial aircrafts the base flow of the EUROTRANS project (see Arnal 1996) has been selected. Within this project, the flow on the fin of the medium-range aircraft Airbus A320 has been measured and documented with the purpose of providing a database open to the scientific community.

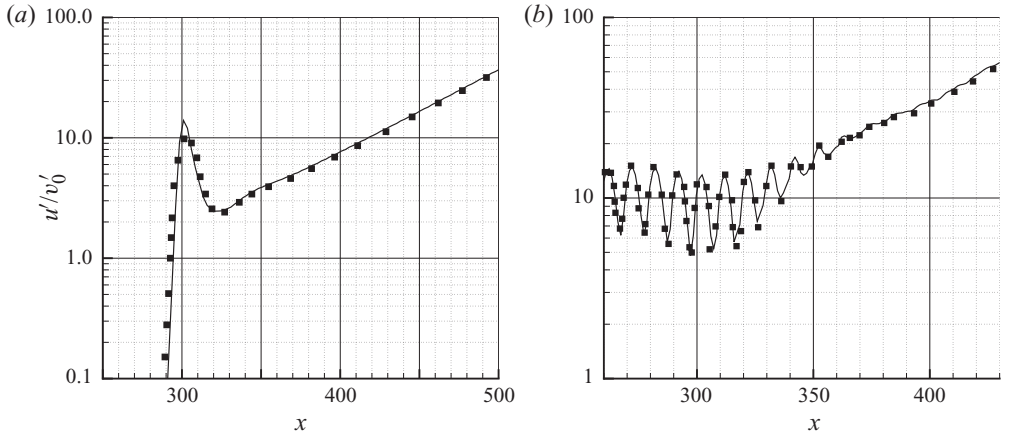


FIGURE 4. Comparison of maximal streamwise velocity disturbance component with numerical results of Spalart (1993) (symbols) for (*a*) a single row of suction holes (figure 2 in Spalart 1993) and (*b*) an array of suction holes (figure 3 in Spalart 1993) in the swept Hiemenz flow.

### 3.1. *Falkner–Skan–Cooke base flow*

For the present simulations the Hartree parameter is $\beta_H = 0.5$ and the sweep angle is $\overline{\varphi} = 45°$. The chordwise free-stream velocity, the kinematic viscosity and the reference length have been set to $\overline{U}_\infty = 159\,\mathrm{m\,s^{-1}}$, $\overline{\nu} = 1.5 \times 10^{-5}\,\mathrm{m^2\,s^{-1}}$ and $\overline{L} = 9.434 \times 10^{-3}\,\mathrm{m}$; thus, $Re_L = 10^5$. The integration domain starts at $x_0 = 2.08559$ and extends 67.45 mm downstream. Within this integration domain, the streamwise free-stream velocity $u_{B,e}$ increases by about 54 %, and therefore the local angle of the potential streamline relative to the chordwise direction decreases from $\overline{\varphi}_e(x_0) = 45°$ at the inflow boundary to $\overline{\varphi}_e(x_n) = 33°$ at the outflow boundary. The displacement thickness based on the chordwise velocity at $x_0$ is $\overline{\delta}_1(x_0) \approx 43\,\mu\mathrm{m}$, which is about half the hole diameter $\overline{d}_H = 100\,\mu\mathrm{m}$ in the subsequent simulations. The Reynolds number based on the displacement thickness increases from $Re_{\delta_1}(x_0) = 450$ to $Re_{\delta_1}(x_n) = 1066$. As the boundary-layer velocity profiles of an FSC flow are self-similar, the shape factor $H_{12}$ takes the constant value of 2.297. The maximum over $y$ of the CF $w_{s,B}$ continuously increases downstream and reaches its maximum of 13.5 % of the streamwise free-stream velocity at the outflow boundary. The properties of the FSC base flow are shown in figure 5.

Primary instability is analysed by means of spatial linear stability theory. The instability region of the FSC base flow for steady modes $\omega = 0$ is shown in figure 6. At the inflow boundary, steady modes with spanwise wavenumbers between $\gamma = 17$ and $\gamma = 137$, corresponding to spanwise wavelengths $433\,\mu\mathrm{m} \leqslant \overline{\lambda}_z \leqslant 3487\,\mu\mathrm{m}$ or $10 \leqslant \lambda_z/\delta_1(x_0) \leqslant 81$, are amplified. The most amplified mode at the inflow has $\overline{\lambda}_z \approx 850\,\mu\mathrm{m} (\gamma \approx 70)$. In the streamwise direction the instability region moderately narrows accompanied by decreasing amplification rates. A typical property of three-dimensional boundary layers is the varying directions of disturbance-wave propagation at successive chordwise locations. Downstream of the stagnation point the flow accelerates, causing a decreasing angle of the potential streamline relative to the chordwise direction. As the wave vector of unsteady and steady amplified disturbances $\boldsymbol{k} = (\alpha_r, \gamma)^T$ is approximately perpendicular to the potential streamline with deviations of a few degrees, its direction gradually moves towards the spanwise direction. This characteristic of the three-dimensional boundary layer is also reflected

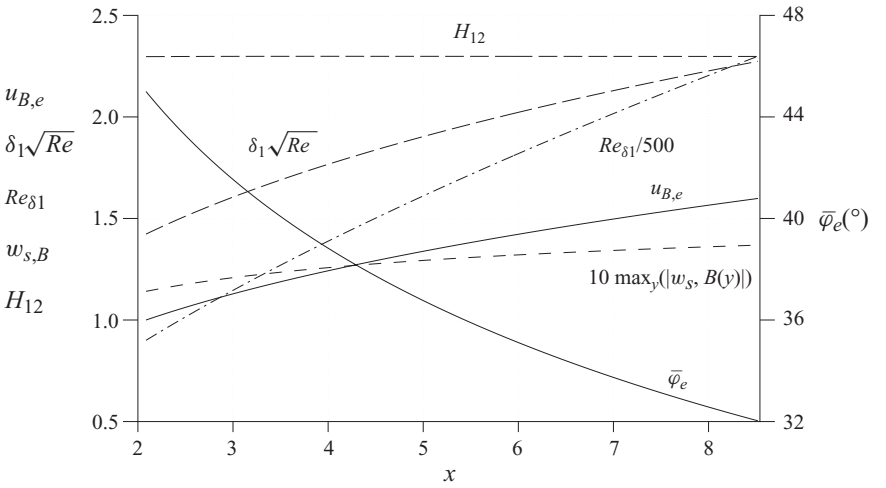


FIGURE 5. Boundary-layer parameters of the investigated FSC base flow.

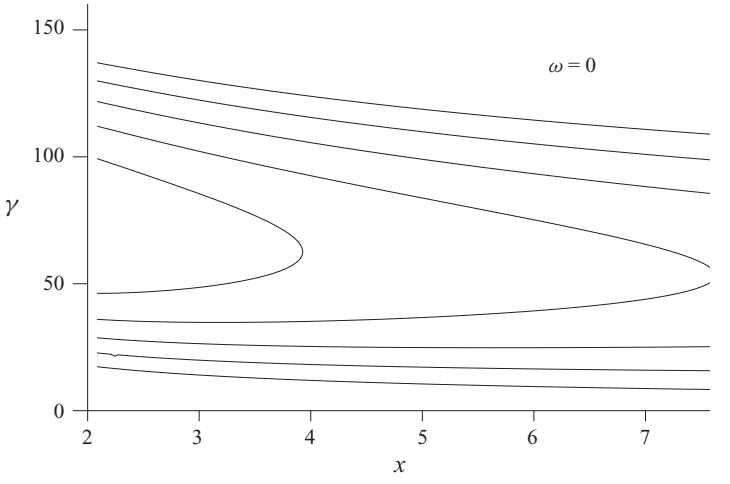


FIGURE 6. Stability diagram for steady disturbances $\omega = 0$ according to linear stability theory for the investigated FSC base flow; growth rate $-\Delta\alpha_i = -0.5$ starting with the neutral curve.

in figure 7. For a constant spanwise wavenumber $\gamma$ the modulus of the chordwise wavenumber $|\alpha_r|$ continuously reduces downstream. Thus, the principle of disturbance cancellation by a staggered suction-orifice order will not work as in two-dimensional boundary layers where steady three-dimensional disturbances are damped eigenmodes. Principally, the approach of disturbance cancellation can likewise be adapted to three-dimensional boundary layers but necessary procedures, as for example proposed by Bertolotti (2003), are sophisticated; see the discussion in § 1. Moreover, this method is so far not proven to give satisfactory results for suction rates $c_q > 0.0001$, which are necessary to stabilize the boundary-layer flow, and is in any case very sensitive to off-design conditions.

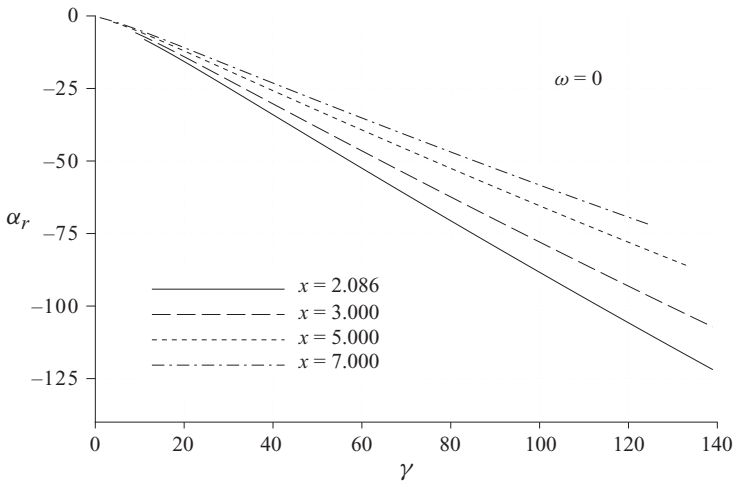


FIGURE 7. Dispersion relation for steady modes at different streamwise locations of the investigated FSC base flow.

### 3.2. *EUROTRANS base flow*

The base flow is the flow past the A320 vertical fin, as available from the EUROTRANS project (Arnal 1996). The free-stream velocity $\overline{U}_\infty = 183.85\,\mathrm{m\,s^{-1}}$, the kinematic viscosity $\overline{\nu} = 3.47 \times 10^{-5}\,\mathrm{m^2\,s^{-1}}$ and the reference length $\overline{L} = 4 \times 10^{-4}\,\mathrm{m}$. The original data were supplied in a conical coordinate system and were then projected onto our Cartesian coordinate system. The free-stream-velocity distribution showed some scatter and had to be smoothed to facilitate stability and DNS. The integration domain begins at $x_0 = 70$, 2.8 cm downstream of the stagnation line, and ends at $x_N = 500$, covering a length of 17.2 cm on the fin. At the inflow plane, FSC velocity profiles with a shape factor $H_{12}$ gained from the given boundary-layer solution were used. The shape factor is $H_{12} = 2.32$ at the inflow boundary and weakly rises up to $H_{12} = 2.41$ at $x_0 \approx 160$, where it stays constant for the rest of the integration domain. The local Hartree parameter of a 'virtual' FSC flow would be roughly $\beta_H \approx 0.4$ at the inflow boundary and $\beta_H \approx 0.2$ downstream of $x_0 \approx 160$. The angle of the potential streamline decreases from $\overline{\varphi}_e(x_0) = 46^\circ$ to $\overline{\varphi}_e(x_n) = 37^\circ$. The maximum CF component reaches its maximum of about 9.3 % at the inflow and continuously declines to 6.1 % at the outflow. The most important parameters of the EUROTRANS base flow are summarized in figure 8.

The resulting stability diagram for steady modes $\omega = 0$ is shown in figure 9 and reflects the strong stability variation which the boundary-layer flow undergoes in the streamwise direction. While the spanwise wavelength range of amplified steady CF modes extends from $800\,\mu\mathrm{m} \leqslant \overline{\lambda}_z \leqslant 4740\,\mu\mathrm{m}$ at $x = 70$, it shifts to $1850\,\mu\mathrm{m} \leqslant \overline{\lambda}_z \leqslant 19\,330\,\mu\mathrm{m}$ at $x = 500$. The value of the locally most amplified mode increases almost by a factor of 2.5 from 1480 μm to $\overline{\lambda}_z(x = 500) = 3590\,\mu\mathrm{m}$. Any control strategy has to take into account this instability variation to ensure an extensive region of laminar flow.

## 4. Discrete steady suction and disturbance excitation

The laminar three-dimensional boundary-layer flow is unstable with respect to steady disturbances which can be excited by distributed discrete suction at the wall. Therefore, we study the excitation spectra of suction-velocity distributions and the

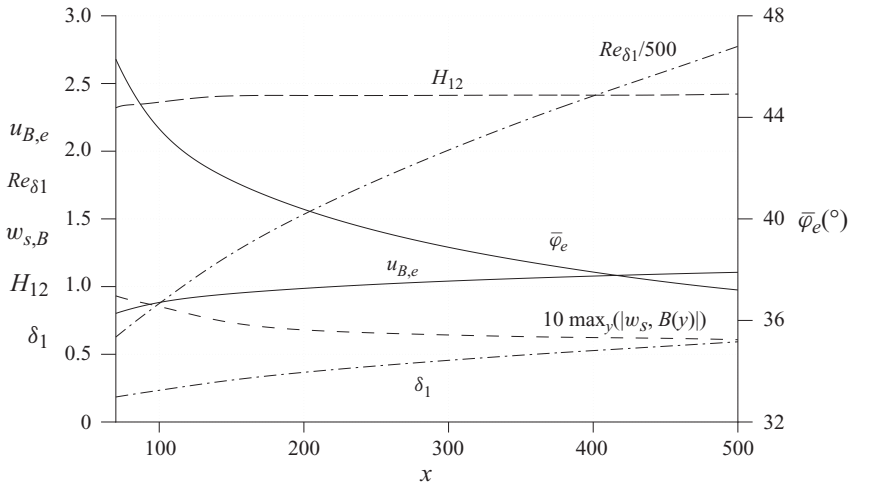


FIGURE 8. Boundary-layer parameters of the EUROTRANS base flow.

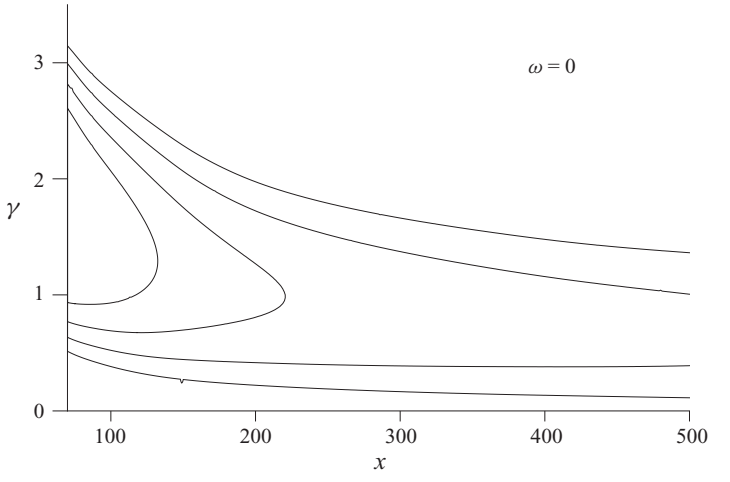


FIGURE 9. Spatial amplification rates $\alpha_i$ of steady disturbances $\omega = 0$ according to linear stability theory for the EUROTRANS base flow; $-\Delta\alpha_i = -0.01$ starting with the neutral curve.

influencing parameters before investigating effects connected to boundary-layer physics, such as receptivity, linear and nonlinear disturbance development, and primary or secondary instability. Relevant parameters affecting the excitation spectra are, on the one hand, the geometry of the suction orifices (e.g. slots or holes), and on the other hand, the distribution of the suction orifices on the surface: spanwise and chordwise spacings, the orifice order and the porosity, which is the ratio of open to total surface area. The influence of the suction-velocity profile over the orifice itself is weak since the induced wavenumbers are large, and suction is less critical than blowing. First, a one-dimensional Fourier analysis in the spanwise direction is applied to analyse the influence of the orifice geometry and, in particular, for holes, the effects of the hole diameter and spanwise suction-velocity inhomogeneities. For a suction panel with successive spanwise rows of holes, the Fourier analysis is extended to the chordwise direction.

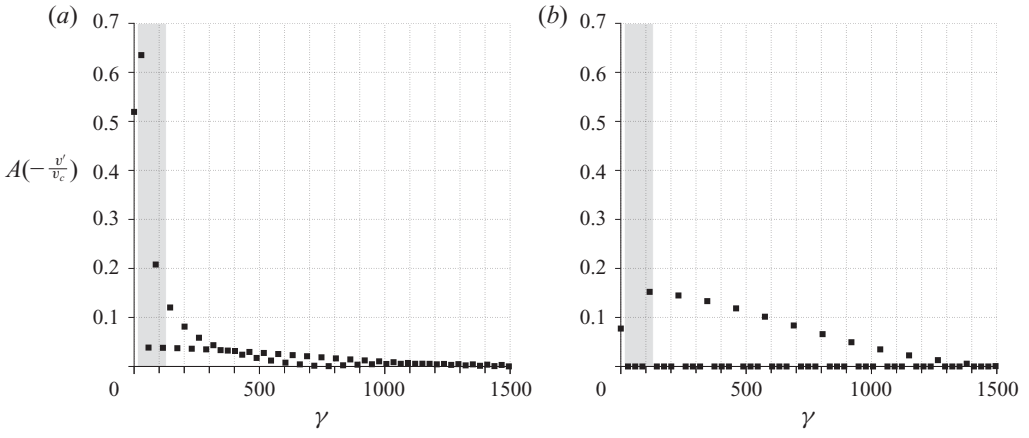


FIGURE 10. Discrete Fourier spectra for the non-dimensionalized disturbance velocity amplitude $(v'/v_c)$ at the spanwise centreline of the disturbance strip for $(a)$ a slot and $(b)$ a row of holes according to figure 3. The grey area indicates unstable spanwise wavenumbers according to spatial linear stability theory for the investigated FSC base flow at $x = 3.06$.

The most simple case is a constant suction-velocity profile along the span in a slit only causing a non-zero Fourier amplitude for the spanwise wavenumber $\gamma = 0$. This mode, however, is in any case the representative of the 'effective' suction exerting a favourable influence on the stability of the laminar flow. For varying suction distribution along the span, modes with $\gamma > 0$ are excited, whose integral over the span is zero, meaning that they will certainly have no stabilizing effect if they are not nonlinearly large. These steady modes with $\gamma > 0$ are dangerous, as they are possibly completed to instability modes amplified by primary instability, depending on the base flow and their spanwise wavenumbers. The excitation of three-dimensional disturbances mainly depends on the porosity. Regarding spanwise slots, as shown in figure 3, with a slot core length half the slot spacing ($\approx 50\,\%$ porosity), only the fundamental mode ($\gamma_0 = 28.75$), corresponding to the spanwise slot spacing, possesses a significant amplitude (see figure 10). For odd multiples of the fundamental mode the amplitude rapidly decays, as for even multiples only the disturbance excitation is present, owing to the circular roundings at the lateral ends of the slots. For a pure rectangular suction-velocity profile with this 50 % porosity, the Fourier amplitudes are analytically given by $A = 2\sin(\gamma L_{SL}/2)/(\gamma L_{SL}) = 2\sin(n\pi/2)/(n\pi)$, $\gamma = n\pi/L_{SL}$, $n = 1, 2, \ldots,$ yielding vanishing amplitudes for even multiples $n = 2, 4, 6, \ldots$. For such slots most of the energy is accumulated in the modes $\gamma = \gamma_0$. With decreasing porosity the energy is successively shifted to three-dimensional modes. The excitation spectra expands, and the decline towards high-wavenumber disturbances is weaker (cf. figure 10$b$). Up to now a regular hole order with constant hole diameter $d$, constant spanwise spacing $s_z$ and constant volume rate per hole $\dot{V}$ are assumed. In this idealized case modes corresponding only to the spanwise hole spacing $s_z$ and its higher harmonics are excited; all other modes vanish. Recall that the suction velocity $v'$ is non-dimensionalized by its maximum $v_c$ at the slot centreline, or at the hole centre. Therefore, for comparisons at equal average suction rates, the spectrum for the hole row in figure 10($b$) has to be multiplied by the amplitude ratio of the wavenumbers $\gamma = 0$ of the cases, here 6.7. The grey areas in figure 10 mark the unstable wavenumber range according to linear stability theory for the FSC base flow at $x = 3.06$. Taking the row of holes, there is still one non-zero amplitude in the instability region, because the spanwise spacing of the holes $s_z$ is still somewhat larger than the smallest wavelength of unstable disturbances at

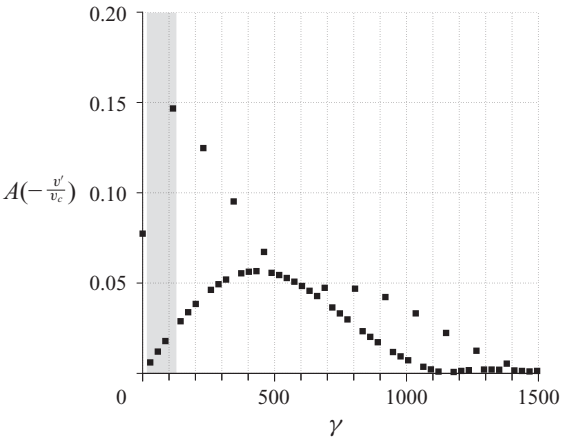


FIGURE 11. Discrete spectrum of Fourier amplitudes as for figure 3(*a*), but one hole has a lateral offset of $0.1s_z$.

this streamwise location. By choosing spanwise spacings smaller than the smallest unstable wavelength, an 'ideal' configuration without forcing of primarily unstable disturbances can theoretically be realized. In practice, inhomogeneities in the suction-velocity distribution are omnipresent. Either hole diameters or hole spacings vary owing to manufacturing imperfections or inhomogeneities occur during operational service of the aircraft by partial clogging of holes. In order to demonstrate the impact of suction inhomogeneities one hole of the configuration in figure 3 is positioned out of order by a lateral shift of $0.1s_z$. Now, the Fourier analysis reveals that all discrete wavenumbers inside the instability region are non-zero (see figure 11). This means that even a clever choice of the spanwise spacing can typically not prevent the excitation of primary unstable disturbances.

These spectra are also important for the spanwise discretization in the numerical simulations. Slots can be realized with fewer spanwise modes, but in any case the de-aliased approach is used. The perforation pattern is Fourier-analysed with a sufficiently large numbers of modes, where the modes with wavenumbers higher than $kmax \times \gamma_0$ in ansatz (2.1) are omitted.

So far a simplified approach has been adopted to investigate excitation spectra by using a one-dimensional Fourier analysis in the spanwise direction. For suction panels this analysis has to be extended to two dimensions, by adding the Fourier transform in the chordwise direction. For illustration we analyse a hole array consisting of 35 hole rows with equal chordwise spacing $s_x = s_z$, where the suction at the first and last rows has been shut off to investigate the effect of non-regularly spaced or finite panels (see figures 12 and 13). Each of the 33 active spanwise hole rows corresponds to the above-discussed hole row with the one-hole offset. For instance, taking the plane at $\alpha_r = 0$, the excitation spectrum of the single row according to figure 11 is obtained. This spectrum repeats every $\Delta\alpha_r = 115$ corresponding to the chordwise spacing of the hole rows. In physical space this means that, starting from one fixed hole, vectors to any other hole of the panel are described. Additionally, the spanwise–chordwise wavenumber spectrum shows that all chordwise wavenumbers are excited for the discrete wavenumbers $\gamma = n \times \gamma_0 = n \times 28.75$ $(n \in \mathbb{N})$, a result of the finite extent of the hole array in the chordwise direction (see figure 13). Thus, suction panels typically excite exponentially growing eigenmodes due to imperfections and/or finiteness.

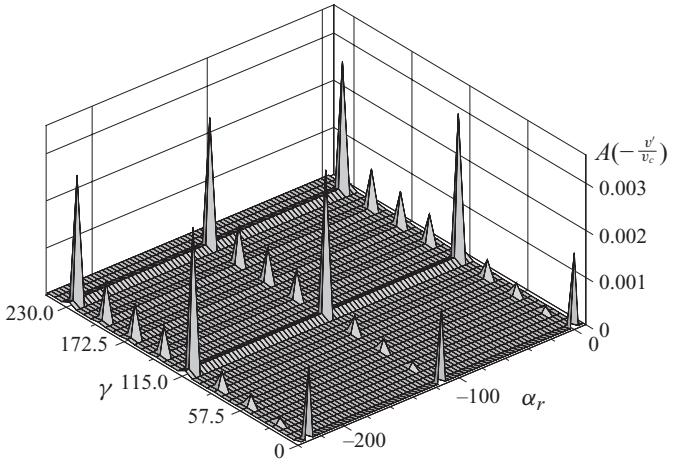


FIGURE 12. A discrete Fourier amplitude spectrum for the non-dimensionalized disturbance velocity $v'/v_c$ over the streamwise ($\alpha_r$)–spanwise ($\gamma$) wavenumber plane for hole array that is finite in the $x$-direction.

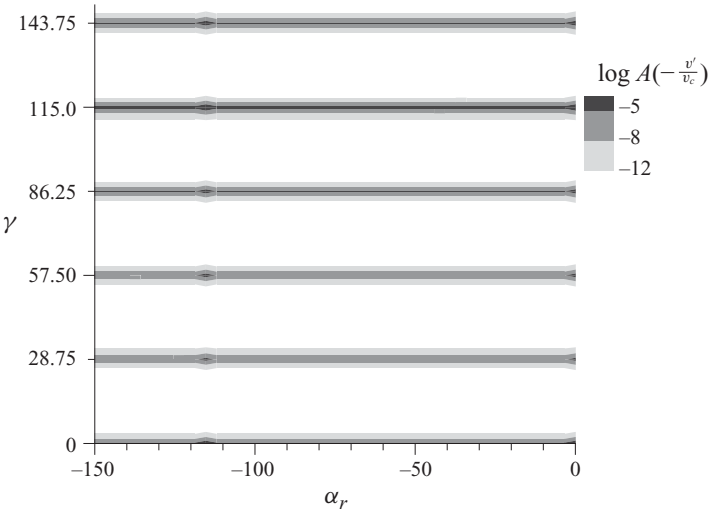


FIGURE 13. As figure 12 but contour lines of the Fourier amplitude spectrum.

## 5. Results for conventional suction

After studying the excitation spectra properties, this section deals with the downstream development of suction-induced disturbances in three-dimensional boundary layers. DNS is particularly suitable for such kinds of investigations as all physical mechanisms that occur are captured, such as the three-dimensional disturbance excitation by spatial discrete suction, receptivity, linear and nonlinear spatial disturbance development, and potentially occurring convective or absolute secondary instability. This section is divided into three parts, consecutively treating the cases of homogeneous suction, 'undercritical' and 'overcritical' suction. In this context undercritical suction means that the use of suction does not cause a premature transition, whereas for overcritical suction or 'oversuction', this is the case. Obviously, the occurrence of oversuction is strongly related to the local suction rate, i.e. to the

| Case | CF-vortex | Homog-low/-high | Oversuction | Forms |
|---|---|---|---|---|
| $\overline{U}_\infty$(m s$^{-1}$) | 159 | 159 | 159 | 183.8 |
| $\overline{L}$ (m) | $9.434 \times 10^{-3}$ | $9.434 \times 10^{-3}$ | $9.434 \times 10^{-3}$ | $4 \times 10^{-4}$ |
| *mmax* | 121 | 121 | 345 | 193 |
| *nmax* | 3601 | 3601 | 11 376 | 9801 |
| *kmax* | 5 | 5 | 47 | 21 |
| $\gamma_0$ | 57.5 | 57.5 | 28.75 | 0.4 |
| $\overline{\lambda}_z$ (μm) | 1031 | 1031 | 2062 | 6283 |
| $\Delta x$ | $1.53 \times 10^{-3}$ | $1.53 \times 10^{-3}$ | $0.628 \times 10^{-3}$ | 0.05 |
| $\Delta y_{min}$ [a] | $0.12 \times 10^{-3}$ | $0.12 \times 10^{-3}$ | $0.642 \times 10^{-4}$ | $0.6 \times 10^{-2}$ |
| $\Delta z$ [b] | $0.11 \times 10^{-1}$ | $0.11 \times 10^{-1}$ | $0.232 \times 10^{-2}$ | 0.341 |
| $\Delta t$ | $0.31 \times 10^{-3}$ | $0.31 \times 10^{-3}$ | $0.105 \times 10^{-3}$ | $0.14 \times 10^{-1}$ |
| $v_c$ | – | $0.71/1.42 \times 10^{-3}$ | 0.11 | 0.0305 |
| $v_m$ | – | $0.71/1.42 \times 10^{-3}$ | 0.0238 | 0.012 |
| $P$ | – | 1 | 0.026 | 0.042 |
| $c_q$ | – | $0.5/1 \times 10^{-3}$ | $0.62 \times 10^{-3}$ | $0.5 \times 10^{-3}$ |
| $\overline{s}_x$ (μm) | – | – | 592 | 1900–2200 |
| $\overline{s}_z$ (μm) | – | – | 515 | 1570 |
| $\overline{d}$ (μm)[c] | – | – | 100 | 160 |

[a] Smallest step size at the wall.
[b] $\Delta z = 2\pi/(2 \times kmax \times \gamma_0)$
[c] Denotes $\overline{d}_H$ or $\overline{d}_{SL}$

TABLE 1. Simulation cases.

momentum of the sucked flow. The stronger the local maximum suction velocity is, the more probable is oversuction. In the following we refer to suction-panel configurations typically in use on actual test demonstrators. The suction orifices, basically suction holes, are aligned in the chordwise direction and can be regarded as isolated disturbance sources that do not directly interact with laterally adjacent suction holes. This is an important point as the work by Goldsmith (1957) treated the problem of a row of closely spaced suction holes in a pipe flow. In this case the physical mechanisms causing oversuction are of a different physical nature.

### 5.1. *Principal effects of suction*

#### 5.1.1. *Homogeneous suction*

The case of a steady and spatially constant suction-velocity distribution is called homogeneous suction. For a given suction rate the best classical stabilization of a boundary-layer flow with respect to steady and unsteady disturbances is achieved by homogeneous suction. Therefore, it can be used as a benchmark to assess the performance capability of skin perforation patterns for laminar flow control by suction.

This section reviews principal properties of homogeneous suction. Three DNS investigations have been performed to study the effects of homogeneous suction. In all cases a steady CF mode with a spanwise wavenumber $\gamma = 57.5$ has been excited in a disturbance strip at $x = 2.62$ by suction and blowing. For comparison, a reference case has been computed without suction (suction rate $c_q = 0$, case 'CF-vortex') and two cases of homogeneous suction in $3 \leqslant x \leqslant 5.15$ at the suction rates $c_q = 0.5 \times 10^{-3}$ (the Homog-low case) and $c_q = 1 \times 10^{-3}$ (the Homog-high case). The simulation parameters are given in table 1, where the definition $c_q = v_{av}/U_\infty$ holds; *nmax*, *mmax* and *kmax* are the grid points used in the $x$-, $y$- and $z$-direction, respectively.

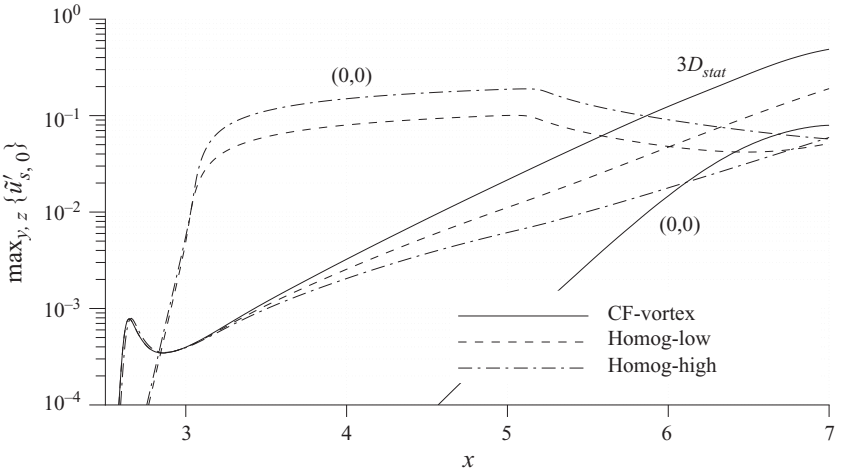


FIGURE 14. $t$-modal amplitude development of the streamwise velocity disturbance along the chordwise direction for steady CF modes ($3D_{stat}$) for single excitation of the vortex mode and homogeneous suction at different suction rates ($\tilde{u}'_s = u'_s/u_{s,Be}$).

Figure 14 shows the amplitude development of the steady disturbances and the mean flow distortion (0,0) for all three cases. (In the following, we mostly present the streamwise or chordwise amplitude development in a streamline coordinate system which is aligned to the potential streamline: see figure 2.) The growth of the CF modes can be significantly attenuated by homogeneous suction. The amplitude of the CF mode $\gamma = 57.5$ at the end of the integration domain reaches approximately $0.5u_{s,Be}$ for the CF-vortex case and is successively reduced to $0.2u_{s,Be}$ and $0.05u_{s,Be}$ for the Homog-low and Homog-high cases. The maximum amplitudes of the mean flow distortion scale with the suction rate and take values of $0.1u_{s,Be}$ and $0.2u_{s,Be}$ at the end of the suction area. Downstream the mode (0,0) continuously declines in the Homog-high case, whereas in the Homog-low case an increase sets in at $x \approx 6.5$. This is due to nonlinear interactions between the three-dimensional modes generating a (0,0)-disturbance part adding to the effect of pure homogeneous suction.

In order to investigate the mean effect of suction on boundary-layer parameters, the velocity profiles and the primary instability, the mode (0,0) of the disturbance flow is added to the base flow. In three-dimensional boundary-layer flows the reduction of the CF by suction is the most important reason for the enhanced stability. Figure 15 shows the maximum CF amplitude for the base flow and the two cases of homogeneous suction. CF permanently decreases as long as suction is active and this reduction scales with the suction rate. The impact of suction on the velocity profiles is shown in figure 16. The shape of the streamwise velocity profile becomes fuller, which is a typical property of homogeneous suction. For $x = 7$ in the Homog-low case, the streamwise velocity profile differs from this characteristic shape. The velocity profile possesses an S-like shape owing to CF vortices which have formed at this streamwise location. For the CF velocity profiles the desired reduction is observed, again scaling with the suction rate. In order to study the effect of homogeneous suction on the growth of unstable disturbances, spatial linear stability theory is applied to the presented velocity profiles. Results of this analysis are shown in figure 17 for steady disturbances $\omega = 0$ and unsteady disturbances with $\gamma = 70$ in figure 18. Basically, homogeneous suction attenuates the growth of unstable disturbances and the damping increases with the

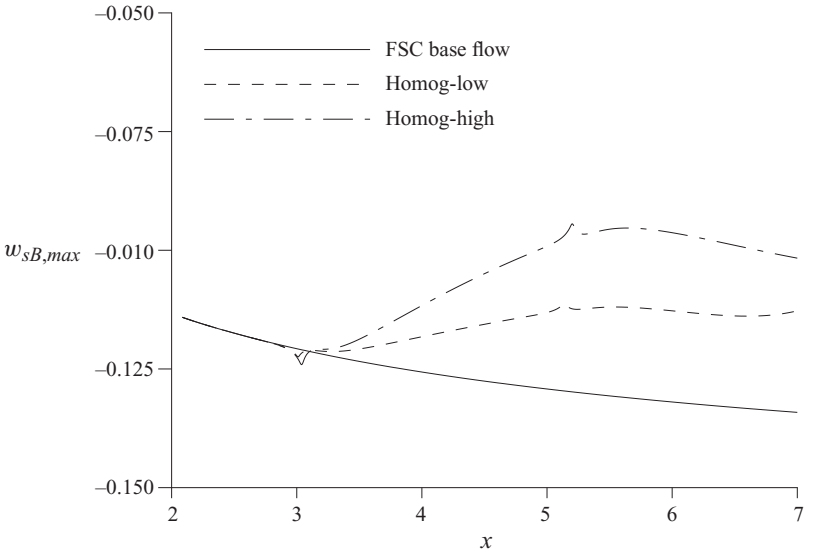


FIGURE 15. Maximum of CF for the investigated FSC base flow and mean flow (base flow + mode (0,0)) for homogeneous suction at different suction rates.

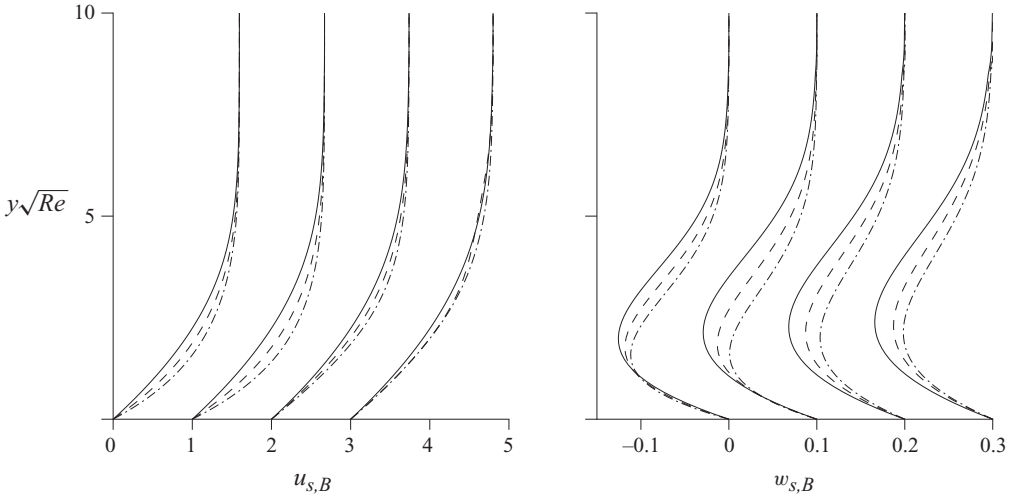


FIGURE 16. Streamwise and CF velocity profiles in a streamline coordinate system of base flow (————) and mean flow (base flow + mode (0,0)) for the Homog-low (– – – –) and Homog-high (– · – · – · –) cases, at different streamwise positions ($x = 4, 5, 6, 7$ from left to right). The abscissa is successively shifted by 1 and 0.1, respectively.

suction rate. For steady disturbances the damping shows strong dependency on the spanwise wavenumber. Large spanwise wavenumbers as well as low spanwise wavenumbers are barely affected by homogeneous suction, as the neutral curve is almost unchanged with or without suction. The best damping is achieved for the most amplified spanwise wavenumbers in the middle of the instability region. However, for unsteady disturbances at a spanwise wavenumber $\gamma = 70$, the damping is nearly independent of the frequency. A remarkable feature can be observed downstream of the suction. Since in the Homog-low case the vortex modes reach higher values first, the accompanying (0,0) generation is also higher, and thus near $x = 7$ the stabilization

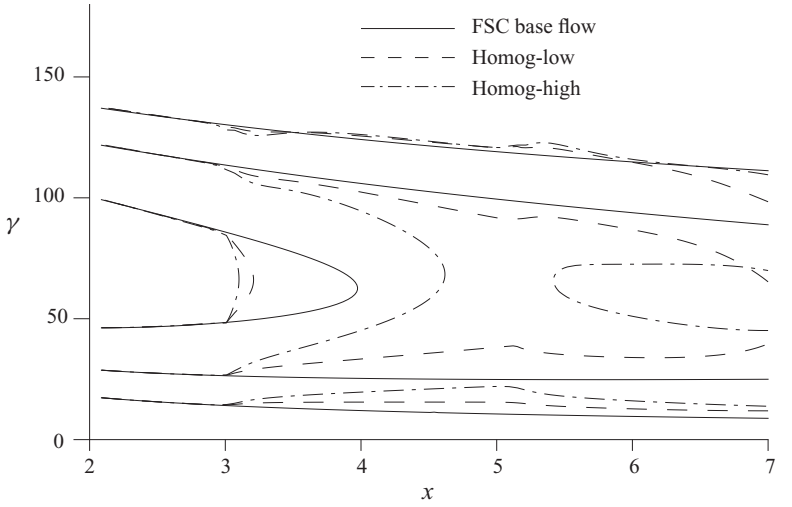


FIGURE 17. Contour lines of spatial amplification rate $\alpha_i$ (starting with the neutral curve $\alpha_i = 0$, $-\Delta\alpha_i = -1$) according to linear stability theory of steady disturbances $\omega = 0$ of base flow and mean flow (base flow + mode (0,0)) of homogeneous suction at different suction rates.

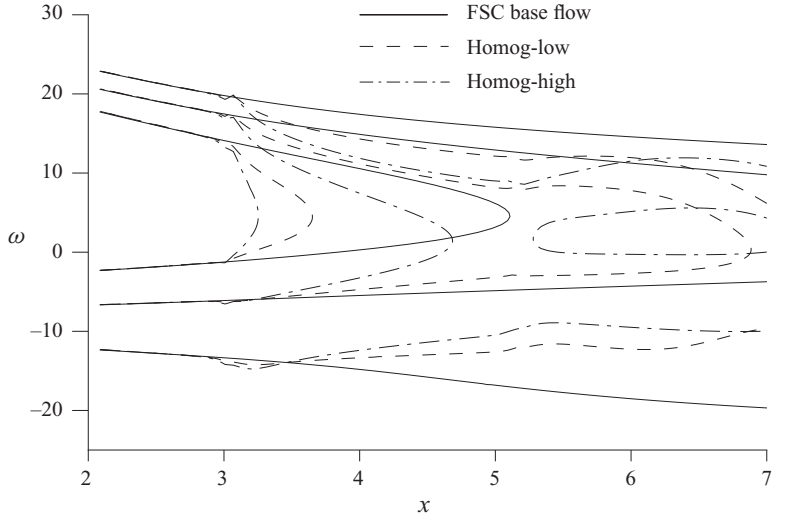


FIGURE 18. The same as in figure 17 but for unsteady disturbances with spanwise wavenumber $\gamma = 70$.

is larger. Thus, large-amplitude vortices may stabilize the boundary layer as long as their three-dimensional deformations do not cause a localized (secondary) instability.

For the Homog-high case the flow again becomes more unstable as the stabilizing suction effect successively fades away, whereas for the Homog-low case this does not hold. On the contrary, the flow is additionally stabilized for steady and unsteady disturbances, despite the fact that the maximum CF amplitude $w_{sB,max}$ is larger for the Homog-low case at an almost equal maximum streamwise velocity $u_{sB,max}$. Additionally, large spanwise wavenumbers are now also damped, which was not the case for pure homogeneous suction. The reason can be found in the different

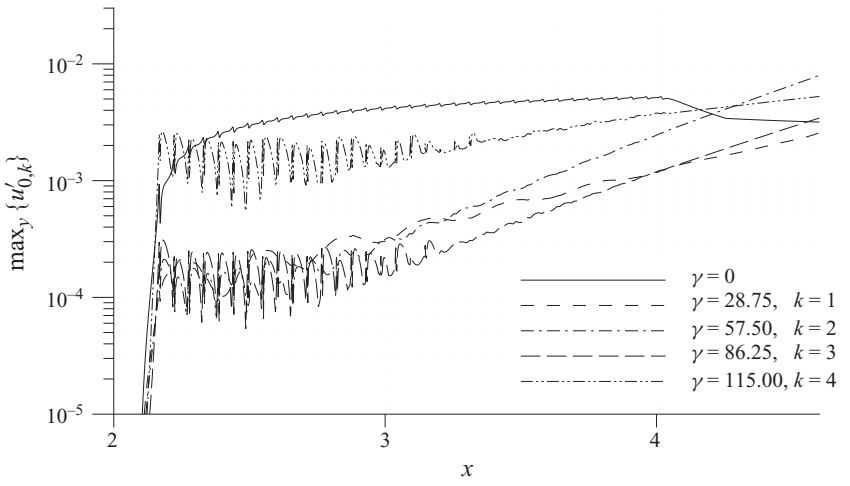


FIGURE 19. $z-t$-modal amplitude development of chordwise velocity disturbance for steady CF modes for a hole array with a streamwise hole row spacing $s_x = 10.28d$ corresponding to a spacing wavenumber $\alpha_r = 115$; $c_q = 0.4 \times 10^{-4}$; 35 hole rows up to $x = 4.02$.

wall-normal velocity distribution at this streamwise location (S-like shape of $u_{sB}(y)$) caused by the CF vortices.

### 5.2. *Generation of crossflow vortex modes by distributed suction*

#### 5.2.1. *Undercritical suction*

A suction panel of 35 identical non-staggered hole rows with $s_x = 10.28d$ and $s_z = 10.3d$ in the FSC base flow is considered, with the suction array extending from $2.17 \leqslant x \leqslant 4.02$. The hole diameter $\overline{d}_H = 50\,\mu\text{m}$, and $d_H/\delta_1(x_0) \approx 1.16$. Within one periodicity length $\lambda_z$, four holes are regularly ordered, except one hole which is again out of order by $0.1s_z$ to model a suction inhomogeneity. The suction rate is $c_q = 0.4 \times 10^{-4}$. In the following the disturbance development within the boundary layer is presented in the frequency-spanwise wavenumber spectrum $(\omega, \gamma)$ or in the frequency spectrum $(\omega)$, showing the maximum amplitudes of the chordwise velocity over the wall-normal direction $y$, respectively the maximum over the wall-normal and spanwise direction $z$, versus the chordwise direction $x$. Figure 19 shows that the mean flow distortion $(0, 0)$ attains a value of 0.5 % of $\overline{U}_\infty$ at the end of the suction array. This value is too small to alter the stability properties of the base flow distinctly. At the very beginning of the suction panel the mode $(0, 0)$ doubles with every successive hole row but soon, downstream, the amplitude increase is reduced. The suction effect of downstream hole rows then just compensates for the decaying suction effect of upstream hole rows. The initial amplitudes of the generated three-dimensional disturbances, further downstream CF modes, scale with their respective excitation amplitudes at the wall. Thus, the mode with $\gamma = 115$ corresponding to the spanwise hole spacing has the largest initial amplitude. At first, all modes oscillate around their initial amplitude level prior to their exponential growth. This behaviour has already been observed by Spalart (1993). Suction at the wall excites damped modes as well as exponentially growing modes of the discrete eigenmode spectrum. In the vicinity of the suction orifice the modes of the continuous spectrum dominate. Downstream of a transient region the discrete exponentially growing eigenmode part prevails and governs the development. For the present hole array the choice of the

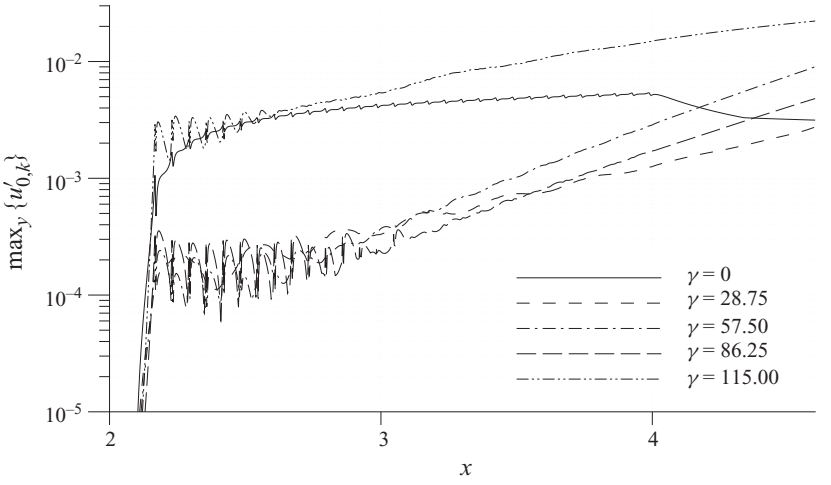


FIGURE 20. As figure 19 but with $s_x = 11.84d$ ($\alpha_r = 100$).

chordwise hole-row spacing $s_x$ is quite favourable as it is small enough not to excite eigenmodes directly (see figure 7): its wavenumber, $|\alpha_r| = 115$, is larger than any chordwise wavenumber of the discrete spectrum of excited modes. The effect of a less careful choice of chordwise hole spacing is shown in figure 20. The spacing has been increased to $s_x = 11.84d$, coinciding with the chordwise wavelength $|\alpha_r| = 100$ of the eigenmode with $\gamma = 115$ at $x \approx 2.2$, meaning that constructive interference between the chordwise hole-row spacing and the wave vector of the discrete eigenmode for the first hole rows can be expected. Now, exponential growth of this mode can be observed, far more upstream than in the previous case, translating into a four-times higher amplitude at $x = 4$, whereas all other modes are barely influenced.

With regard to laminar flow control, the use of the term 'constructive' interference is at first misleading, as the minimization of suction-induced disturbances seems to be the most reasonable design objective. In order to ensure that no constructive interference enhancing amplification of primary unstable modes occurs, the spacing of suction orifices has to be locally smaller than the smallest wavelength component of amplified eigenmodes in each direction. This ensures that any (inevitably) generated higher harmonics are in the safe region of the wavenumber spectrum. Even in an accelerated flow spanwise and chordwise wavelengths of unstable modes increase downstream, meaning that uncritical spacings also increase. This constraint reflects the fact that suction orifices and CF vortices should not be aligned, to avoid constructive interference.

Contrary to this classical way of thinking, the deliberate selective excitation of CF modes by suction orifices offers an option to maintain laminarity of boundary layers dominated by CF instability. Details of this new approach based on the continued UFD technique are presented in § 6.

### 5.2.2. *Overcritical suction*

The key issue for any application using discrete suction to keep the three-dimensional boundary-layer flow laminar is the successful control of the excitation or growth of steady CF modes. As we have seen, this can be achieved by increasing the porosity of the surface which, for many aeronautical applications, e.g. on wings or tailplanes, is unfavourable because of to structural design constraints. Once steady

CF modes are excited they amplify, owing to primary instability, with typically large amplification rates in the leading-edge region. The only way to attenuate the growth and possibly avoid turbulence is an increase of the suction rate to reduce the CF, enhancing the boundary-layer stability. Thus, one may conclude that any boundary-layer flow could be kept laminar if the suction is only strong enough. Indeed, within certain ranges the suction strength and invoked disturbance damping are directly related. However, experience shows that there are limits. Above certain threshold values high localized suction velocities trigger premature transition by oversuction, which cannot be regarded as a unique physical process. First, strong suction by holes always generates vortices and subsequent regions of low velocity at spanwise positions between the holes, giving rise to strong wall-normal and spanwise shear and either spectral or localized secondary instability downstream, also depending on the type of base flow. Second, even stronger suction can lead to flow separation at the hole positions by sucking too much fluid from downstream, causing rapid laminar breakdown. The mechanisms strongly depend on the specific flow conditions.

The experimental work by Goldsmith (1957) and the related more recent numerical studies of Meitz & Fasel (1995) treated closely spaced suction holes, i.e. with $s_z/d_H \approx 2$, in a Blasius boundary layer. For this configuration interactions between adjacent holes of the same hole row dominated the flow. (We note in passing that recent extensive numerical resolution studies using our code have shown that the results presented by Meitz & Fasel 1995 are not converged and that a much finer grid in the wall-normal direction is necessary to correctly resolve suction phenomena at suction velocities higher than about 20 % with the vorticity–velocity code used.) Further work on two-dimensional boundary layers without CF has been done experimentally (Gregory 1961; Reneaux & Blanchard 1992; MacManus *et al.* 1996; MacManus & Eaton 2000), numerically (Müller, Kloker & Bestek 1992; MacManus & Eaton 1996, 2000) and theoretically (Wortmann & Weise 1970) to address the problem of oversuction. In this context a major concern has always been the evaluation of criteria to predict the occurrence of oversuction. Besides the conclusion that this is far from a simple task, considering the wealth of involved parameters (such as hole diameter, hole spacing, hole order or suction rate, just to name a few), it has to be pointed out once more that it seems extremely questionable that a transfer of knowledge to three-dimensional boundary layers is feasible. Again the reason is the CF and its impact on the flow physics.

The emphasis of the following investigations is on the range $5 \leqslant s_z/d_H \leqslant 10$, as these are typical values used in recent flight-test campaigns. Furthermore, the aim is not to postulate new quantitative criteria for oversuction in three-dimensional boundary layers but to provide some fundamental insight into the basic physical mechanisms.

A hole array of 97 hole rows (the oversuction case) is considered to extend from $x = 2.903$ to $x = 8.93$. The hole rows are configured as before (cf. figures 3 and 11), and are spaced at $\overline{s}_x = 592\,\mu\text{m}$ in the chordwise direction. Thus, the porosity of the panel is $P = 0.026$. The suction rate is $c_q = \overline{v}_{m,H} P/\overline{U}_\infty = 0.62 \times 10^{-3}$, with $\overline{v}_{m,H}$ denoting the average suction velocity over a hole, leading to a maximum suction velocity at the hole centre $v_c = 0.11$ for the given porosity. In the DNS the final value of the suction velocity is reached after a prescribed smooth timewise increase within the first 300 time steps ($\approx 0.2$ % of the computed time steps to converge to steady state). Nevertheless, the start-up procedure causes an initial pulse travelling through the integration domain downstream. Only after the pulse has completely passed the outflow boundary does the whole flow field attain a steady state. (We note that careful

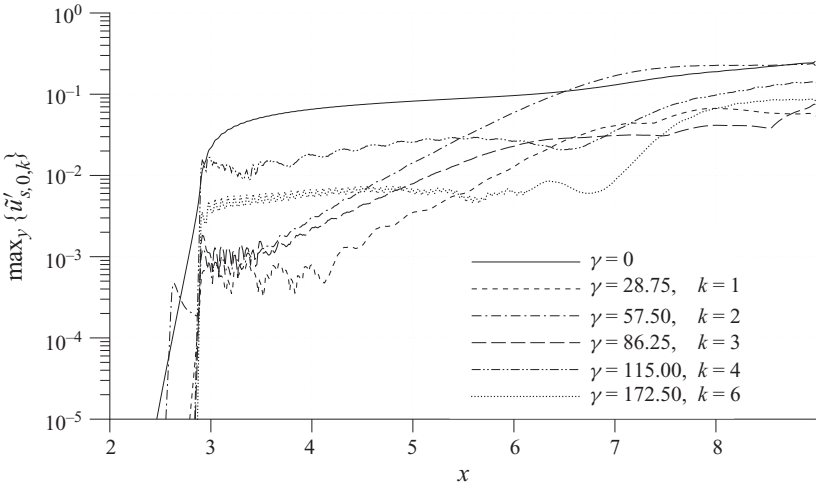


FIGURE 21. $z - t$-modal amplitude development of streamwise velocity disturbance in a streamline coordinate system for steady CF modes for the oversuction case. Hole array with 97 hole rows up to $x = 8.93$ and $c_q = 0.62 \times 10^{-3}$: overcritical suction. No forcing of unsteady disturbances.

grid-resolution investigations are mandatory to finally yield grid-independent results.) A double-spectral Fourier analysis of this steady state yields the results plotted in figure 21. The amplitude of the mean flow distortion ($\gamma = 0$) grows monotonically until the end of the domain. Up to $x \approx 6.5$, the growth is mainly due to the pure effect of suction. Downstream of this location a nonlinearly generated contribution of large-amplitude CF modes successively adds to the effect of suction. As the receptivity coefficients for all CF modes are similar, the initial amplitudes in the boundary layer at the beginning of the hole array correlate as in the excitation spectrum at the wall (cf. figure 11). At first, oscillations of the amplitudes can again be observed for all CF modes as in the case at lower suction rates (cf. figures 4 and 19). Exponential growth sets in, and going upstream, the larger the primary amplification rate of the mode. As a result the mode with $\gamma = 57.5$ first saturates, suppressing the growth of the other CF modes except, of course, its higher harmonics, $k = 4, 6, 8, \ldots$. This scenario turned out to be of fundamental significance in all numerical simulations performed. Whatever the details of the perforation pattern, after some streamwise extent the naturally most amplified CF mode always prevails and, in this case, fixes the onset of laminar–turbulent transition if unsteady background disturbances are added.

In order to check whether secondary instability sets in, a pulse-like disturbance is periodically forced simultaneously at $x = 3.57, 4.57, 5.57, 6.57$ after the flow has reached a steady state. The pulse is composed of 15 harmonic waves of equal phase and amplitude. The discrete frequency range extends from $\omega = 20$ to $\omega = 300$, $\Delta\omega = 20$, the spanwise wavenumber being $\gamma = \pm 57.5$ and the forcing amplitude of each component $A_{h,k} = 2 \times 10^{-3}$; cf. (2.7). Figure 22 shows the $t$-modal amplitude development. Downstream of the very first two excitation stations all unsteady modes are damped. After station 3 some modes no longer decay and after station 4 an explosive growth suddenly takes place, particularly of high-frequency modes, leading to a transition from laminar to turbulent flow ($x > 8.5$). The highest amplification rates can be observed initially for the frequencies $120 \leqslant \omega \leqslant 160$, approximately 10 times larger than the primary amplification rate of the most unstable CF mode

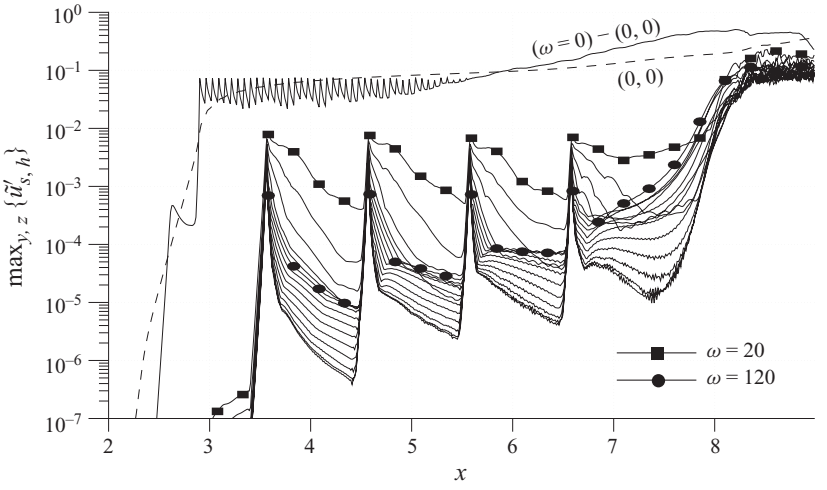


FIGURE 22. $t$-modal amplitude development for the oversuction case with additional forcing of periodic background pulses. Frequencies from $\omega = 20$ to $\omega = 300$, with $\Delta\omega = 20$, are shown. The two-dimensional part of the mean-flow distortion is denoted by (0,0), and its three-dimensional part by $(\omega = 0) - (0, 0)$.

at this downstream location. The observed high-frequency secondary instability is of a convective nature, as Fourier analyses of subsequent periods of the fundamental forcing frequency yield identical results. Therefore, timewise disturbance growth can be excluded, as otherwise indicating absolute/global instability. A better understanding of the physical mechanisms can be gained by visualizations of the vortex structures by $\lambda_2$-isosurfaces, shown in figure 23. For better visibility the integration domain is roughly aligned in the direction of the CF-vortex axis. In figures 23($a$) and 23($b$) zooms of the region of laminar–turbulent transition are depicted at $t/T_0 = 0$ and $t/T_0 = 0.5$ of the fundamental pulsing frequency ($\omega_0 = 2\pi/T_0 = 20$) by a rotation of the plate-fixed coordinate system of 32° at $x_r = 7.3$ and $z = 0$. The coordinates shown correlate with the standard system by $x - x_r = \xi \times \cos(32°) - \zeta \times \sin(32°)$ and $z = \xi \times \sin(32°) + \zeta \times \cos(32°)$. In figure 23($c$) a large part of the integration domain is shown by a rotation of 32° at $x_r = 3.2$ and $z = 0$. Note that suction is also fully active at the downstream ends of the domains shown.

The visualizations confirm the observations that the most amplified eigenmode (0,2) dominates the flow. Two CF vortices form per fundamental spanwise wavelength $\lambda_Z$ which are not exactly equal in strength. Breakdown of the laminar flow is triggered by finger-like vortices wrapping around the stronger CF vortices, a transition scenario which has already been observed in CF-dominated three-dimensional boundary-layer flows without suction (see Wassermann & Kloker 2002). However, we note that laminar breakdown on a steadily active suction panel cannot be anticipated simply, since the deformed primary state differs from the case without suction, especially with respect to the wall-normal velocity, which can influence the secondary instability.

## 6. Formative suction

The main conclusion of the results obtained so far is that a skin perforation pattern should operate at large suction rates to securely stabilize the boundary layer

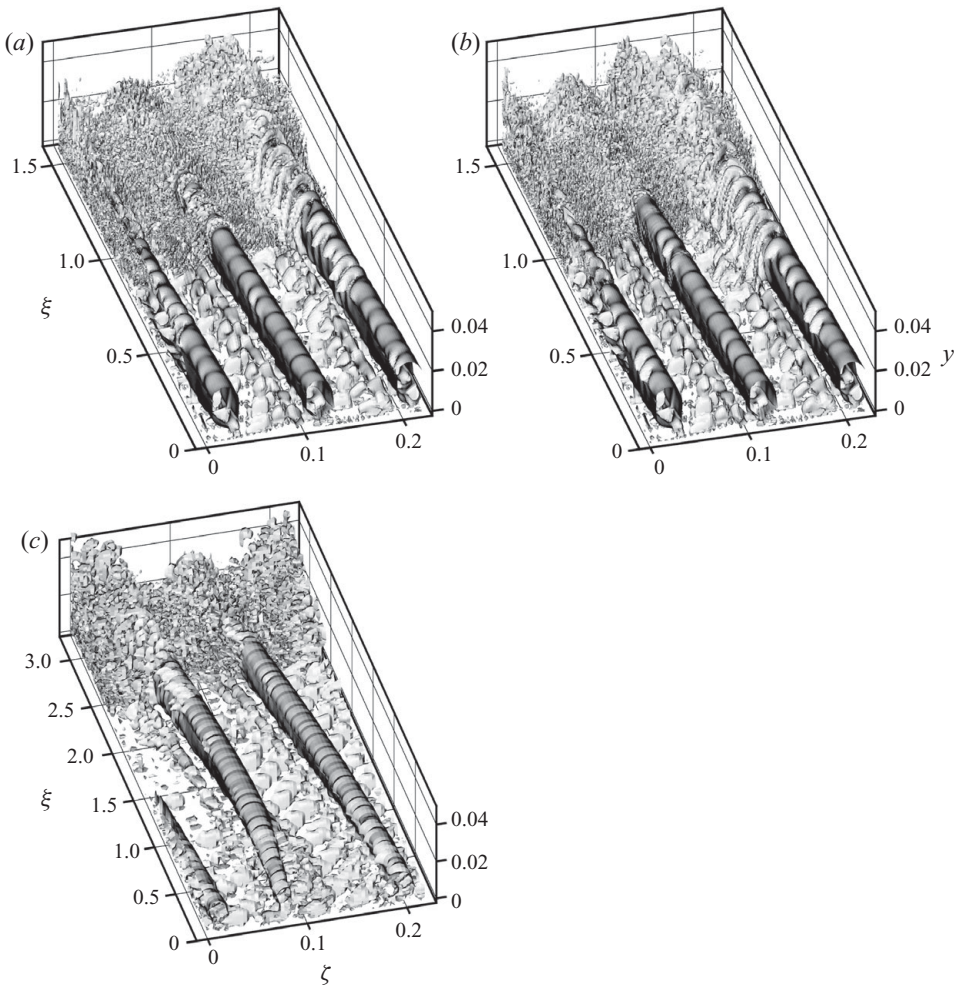


FIGURE 23. Visualization of vortical structures in the instantaneous flow fields for the oversuction case plus periodic background pulses by $\lambda_2$-isosurfaces, $\lambda_2 = -4$, at subsequent times $(a,b)\ t/T_0 = 0, 0.5$ for a zoom of the rear part of integration domain and at $(c)\ t/T_0 = 0$ for a large part of the integration domain. $T_0$ is the period of the pulsing frequency. Approximately one spanwise wavelength is shown in the coordinate system, which is roughly aligned along the CF-vortex axis.

via the two-dimensional mean flow distortion in combination with low excitation of three-dimensional disturbances. These requirements result in perforation patterns, with high porosity not being desirable from a structural point of view. Apart from this, all actions allowing reduction of the suction rate are highly appreciated, as the total energy balance is favourably affected and the pump power can be lowered.

We investigate here an approach combining classical suction with the UFD method (see Wassermann & Kloker 2002). The main idea is to excite benign closely spaced (UFD) vortices and maintain them on a beneficial amplitude level by an appropriate order of suction orifices. The streamwise variation of flow conditions and stability characteristics can be taken into account by adapting the spacing of the suction orifices. In this way we overcome the shortcomings of the single excitation of UFD

vortices, which works well only for non- or weakly varying stability properties. Note, however, that it is not clear *a priori* which direction the vortices follow – the flow direction depends on the wall-normal distance – and improper excitation can lead to nonlinear interactions with nocent vortices. If properly designed, this formative suction unifies the stabilizing effects of boundary-layer suction and UFD. Consequently, a reduction of suction rate for the same degree of stabilization is possible. The forced vortices generate, by nonlinear mechanisms, a mean flow distortion not unlike suction (see Wassermann & Kloker 2002), influencing the stability in a manner just as favourable as suction itself. Compared to the strategy of minimizing the excitation of unstable modes by the perforation pattern, three-dimensional disturbances not generated by the pattern itself can now be suppressed or weakened.

The following simulations (case forms) not only aim at a clarification of the underlying physical effects but should additionally demonstrate the feasibility of the new method in a 'realistic' boundary-layer flow for an extended chordwise distance. Hence, the EUROTRANS base flow has been adopted with a chordwise length of about 17 cm. In order to evaluate the formative suction, simulations of homogeneous suction at equal suction rates have been performed. This constitutes a challenging benchmark, as no practical method so far will perform as well as homogeneous suction.

One step towards an optimized skin perforation pattern is the use of spanwise slots. The slots have a slot width – the extent in the chordwise direction – $\overline{d}_{SL} = 160\,\mu\text{m}$ and a total slot length $\overline{L}_{SL} + \overline{d}_{SL} = 890\,\mu\text{m}$. The slot array extends from $90 \leqslant x \leqslant 513$ in the chordwise direction, with a porosity of 4.2 %. Four slots are regularly ordered laterally within one fundamental spanwise wavelength $\lambda_z$.

The integrally most amplified steady CF mode $\gamma = 0.8$ is disturbed for the purpose of comparison. This is done by suction and blowing in a disturbance strip at $x = 86$. The suction rate is $c_q = 0.5 \times 10^{-3}$. The basic approach of formative suction is now presented for the example of the EUROTRANS base flow. According to the stability diagram of steady CF modes of the undisturbed base flow, the mode $\gamma = 1.6$ is chosen as the UFD mode. Immediately, a major difficulty becomes obvious when tracking downstream the amplification rate $\alpha_i$ (cf. figure 9). At $x \approx 330$ the selected UFD mode is damped according to the primary stability theory, and this will occur even further upstream if a composed base flow is considered where the suction effect is added to the EUROTRANS base flow. Hence, downstream of $x \approx 330$ the mode $\gamma = 1.6$ is no longer expected to serve as a UFD mode, and further steps need to be undertaken. The use of an adapted perforation pattern to meet this requirement is, of course, possible. The slots are aligned parallel to the leading edge and are spaced at $\overline{s}_z = 1570\,\mu\text{m}$ in the spanwise direction to produce a peak amplitude in the excitation spectra at $\gamma = 1.6$. In the chordwise direction the slot rows are spaced at a regular distance of $\overline{s}_x = 2200\,\mu\text{m}$ for the first five slot rows, and then the chordwise spacing is continuously adapted to match the chordwise wavelength $\alpha_r$ of the eigenmode $\gamma = 1.6$ of the undisturbed laminar base flow precisely. Figure 24 shows how the steady CF modes develop for such a configuration. The intentionally excited mode $\gamma = 1.6$ already serving as the UFD mode has an initial amplitude of 2 %–3 % at the first slot rows. As the adaptation of the chordwise spacing is not immediately imposed at the first rows, exponential growth does not prevail before the 12th slot row, $x = 145.65$. The mode saturates at an amplitude of 19 % around the 37th slot row, $x = 270.6$. Downstream the mode is again damped to an amplitude level of around 5 % where it stays nearly constant until the end of the domain. The benefit can be seen in the amplitude development of the mean flow distortion ($\gamma = 0$) and the most

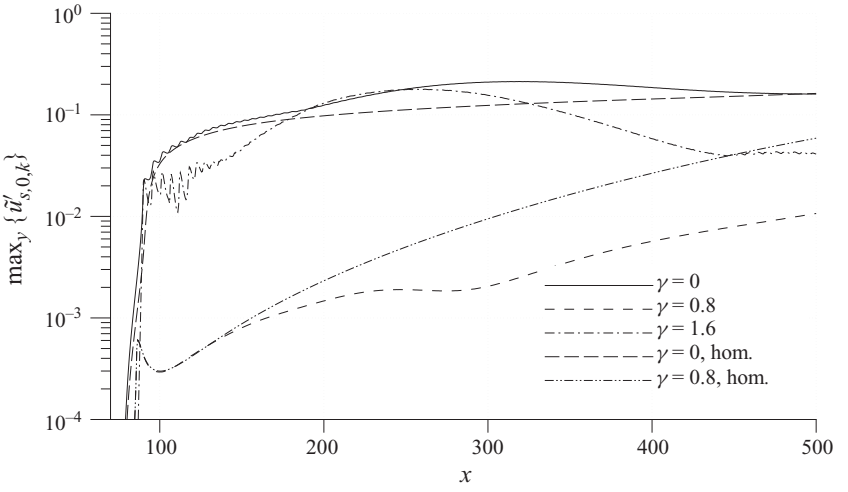


FIGURE 24. $z-t$-modal amplitude development for steady CF modes for the case of forms and homogeneous suction at equal suction rate (abbreviation hom.).

amplified mode $\gamma = 0.8$, in comparison with the respective amplitude development when homogeneous suction is applied. The UFD mode $\gamma = 1.6$ increasingly reveals its favourable impact and nonlinearly generates a noticeable contribution to the mean flow distortion $\gamma = 0$. The maximum of this contribution is shifted downstream relative to the maximum of the UFD vortices. At the end of the considered slot array the influence of the UFD mode virtually vanishes as it is damped, and the amplitude of $\gamma = 0$ again approaches the homogeneous suction case. The amplitude development of the selected test mode $\gamma = 0.8$ finally shows the desired effectiveness of the formative suction. Except for the region close to the excitation location, the test mode undergoes a stronger damping throughout the entire integration domain. The damping attains its maximum where the UFD vortices reach maximum amplitudes. For this specific case the use of formative suction reduces the amplitude of the most dangerous CF mode $\gamma = 0.8$ by a factor of approximately 6.

Of course, imposing CF vortices is a delicate procedure, as the danger of turbulence triggered by secondary instability is always present. Once more a pulse is forced at $x = 185$ to check for secondary instabilities. The result of this verification is plotted in figure 25. No onset of secondary instability is observed.

## 7. Conclusions

Spatial DNS investigations have been carried out to investigate the effects of discrete suction holes at the wall on the disturbance evolution in laminar three-dimensional boundary-layer flows with favourable pressure gradients. The main conclusions are as follows.

(i) Weak to moderate suction through a hole locally induces a counter-rotating streamwise vortex (mode) pair in the near field downstream of the hole, such that both transport fluid into the hole. The vortex that is consistent with the instability motion induced by the CF shear-layer – transporting fluid near the wall in the CF direction – is supported; the other vortex is suppressed.

(ii) Suction panels can exponentially excite growing vortex eigenmodes even if the nominal spanwise/chordwise orifice spacing is subcritical, i.e. smaller than the

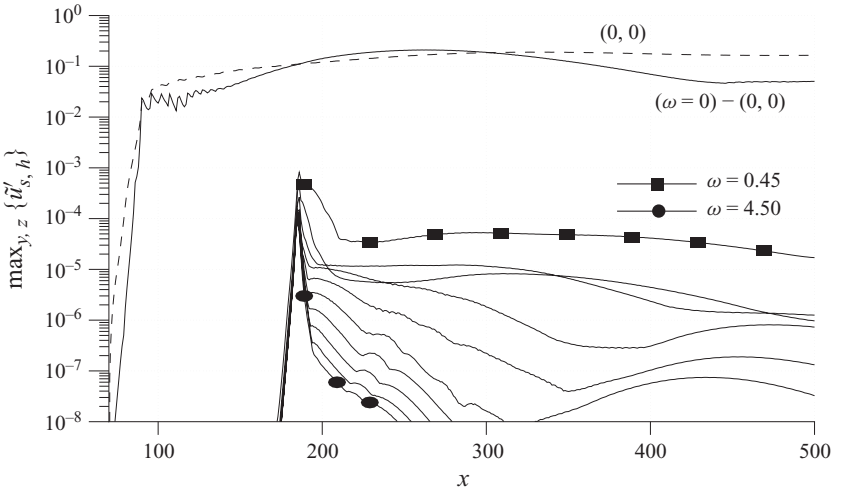


FIGURE 25. $t$-modal amplitude development for the case of forms with forcing of periodic background pulses.

respective wavelength of amplified modes, owing to imperfections in the hole positions or sizes, or suction strength, and the finite chordwise extent of the suction area. Of course, the mean suction effect attenuates the growth compared to the case without suction. But for randomly perforated panels it is very likely that the naturally most amplified steady CF mode will prevail, eventually bounding the laminar-flow range by generating large-amplitude CF vortices and their secondary instability.

(iii) Secondary instability sets in even on an active suction panel. It is generally not inhibited by the alteration of the wall-normal velocity component by distributed suction. (Very strong and localized ('pinpoint') suction can weaken the instability.)

(iv) A CF-vortex mode can deliberately be excited and forced by matching the spanwise and chordwise suction orifice spacing to its wave vector. If this mode is amplified by instability its excitation in the first part of the panel is decisive. However, further downstream, support by adapted increase of the chordwise orifice spacing, to account for the wave vector alteration due to the evolving mean flow, can make significant contributions. Moreover, the suction strength can be adapted. If the forced mode is chosen with less than two-thirds of the most amplified spanwise wavelength and reaches a large amplitude, all modes that are not higher harmonics are nonlinearly suppressed, and the resulting dominating vortices do not cause significant secondary instability. In the case shown, this formative suction, based on a mode with one half of the most amplified spanwise wavelength, lowers the amplitude of a nocent steady test mode by a factor of 6 on a distance of about 450 mean boundary-layer displacement thicknesses compared to the ideal homogeneous suction at equal suction rate. Formative suction may also extend the UFD technique originally introduced with a single excitation station (of roughness) to base flows with strong streamwise alterations where multiple excitation rows are mandatory.

(v) We note that standard optimizations of suction, striving for minimization of the suction amount for a prescribed stabilization, have been based so far on the assumption of ideal homogeneous suction not inducing any unstable (CF) modes by definition. Real suction panels with many orifices, however, always give rise to local three-dimensional effects, unless long spanwise slits are used. The method of

minimizing the excitation of nocent modes by grouping the orifices such that the excitation spectrum has low amplitudes at values of amplified eigenmodes yields low disturbances arising from the clean, design panel itself, but has difficulties with an unclean situation. Formative suction could be a remedy.

## REFERENCES


Abegg, C., Bippes, H. & Bertolotti, F. P. 1999 On the application of suction for the stabilization of crossflow instability over perforated walls. In *New Results in Numerical and Experimental Fluid Dynamics* (ed. W. G. Nitsche, H.-J. Heinemann & R. Hilbig), vol. II, *Proceedings of the 11th AG STAB/DGLR Symposium*, Notes on Numerical Fluid Mechanics, vol. 72. Vieweg.

Abegg, C., Bippes, H. & Janke, E. 2000 Stabilization of boundary-layer flows subject to crossflow instability with the aid of suction. In *Laminar–Turbulent Transition* (ed. H. F. Fasel & W. S. Saric), *Proceedings of the IUTAM Symposium*, Sedona 1999. Springer.

Arnal, D. 1996 The EUROTRANS project. In *Proceedings of the 2nd European Forum on Laminar Flow Technology*, Bordeaux, France.

Arnal, D., Seraudie, A. & Archambaud, J. P. 2000 Influence of surface roughness and suction on the receptivity of a swept wing boundary layer. In *Laminar–Turbulent Transition* (ed. H. F. Fasel & W. S. Saric), *Proceedings of the IUTAM Symposium*, Sedona 1999. Springer.

Bertolotti, F. P. 2003 The equivalent forcing model for receptivity analysis with application to the construction of a high-performance skin perforation pattern for LFC. In *Recent Results in Laminar–Turbulent Transition* (ed. S. Wagner, M. J. Kloker & U. Rist), Selected numerical and experimental contributions from the DFG priority programme 'Transition' in Germany, Notes on Numerical Fluid Mechanics, vol. 86, pp. 25–36. Springer.

Bestek, H., Müller, W., Kloker, M. J. & Bieler, H. 1996 Effect of discrete suction strips on the stability of 3D-boundary layers: direct numerical simulation for boundary layer flow modelling. In *Proceedings of the 2nd European Forum on Laminar Flow Technology*, Bordeaux, France.

Bippes, H. 1999 Basic experiments on transition in three-dimensional boundary layers dominated by crossflow instability. *Prog. Aerosp. Sci.* **35**, 363–412.

Bonfigli, G. & Kloker, M. J. 1999 Spatial Navier–Stokes simulation of crossflow-induced transition in a 3-D boundary layer. In *New Results in Numerical and Experimental Fluid Dynamics* (ed. W. G. Nitsche, H.-J. Heinemann & R. Hilbig), vol. II, *Proceedings of the 11th AG STAB/DGLR Symposium, 1998*, Notes on Numerical Fluid Mechanics, vol. 72, pp. 61–68. Vieweg.

Bonfigli, G. & Kloker, M. J. 2007 Secondary instability of crossflow vortices: validation of the stability theory by direct numerical simulation. *J. Fluid Mech.* **583**, 229–272.

Bulgubure, C. & Arnal, D. 1992 Dassault Falcon 50 laminar flow flight demonstrator. In *DGLR-Bericht 92-06*, *Proceedings of the First European Forum on Laminar Flow Technology*, Hamburg, Germany.

Goldsmith, J. 1957 Critical laminar suction parameters for suction into an isolated hole or a single row of holes. *Rep.* BLC-95. Northrop Aircraft.

Gregory, N. 1961 Research on suction surfaces for laminar flow. In *Boundary Layer and Flow Control* (ed. G. V. Lachmann), vol. 2, pp. 924–960, Pergamon.

Joslin, R. D. 1998*a* Overview of laminar flow control. *TP-1998-208705*. NASA Langley Research Center, Hampton, VA.

Joslin, R. D. 1998*b* Aircraft laminar flow control. *Annu. Rev. Fluid Mech.* **30**, 1–29.

Kloker, M. J. 2008 Advanced laminar flow control on a swept wing: useful crossflow vortices and suction. *Paper* 2008-3835. AIAA.

MacManus, D. G. & Eaton, J. A. 1996 Micro-scale three-dimensional Navier–Stokes investigation of laminar flow control suction hole configurations. *Paper* 96-0544. AIAA.

MacManus, D. G. & Eaton, J. A. 1998 Measurement and analysis of the flowfields induced by suction perforations. *AIAA J.* **36** (9), 1553–1561.

MacManus, D. G. & Eaton, J. A. 2000 Flow physics of discrete boundary layer suction: measurements and predictions. *J. Fluid Mech.* **417**, 47–75.

MacManus, D. G., Eaton, J. A., Barrett, R., Rickards, J. & Swales, C. 1996 Mapping the flow field induced by a HLFC perforation using a high resolution LDV. *Paper* 96-0097. AIAA.

MADDALON, D. V. 1991 Hybrid laminar-flow control flight research. *Tech. Rep.* TM-4331, p. 47. Research and Technology, NASA.

MADDALON, D. V., COLLIER, F. S., MONTOYA, L. C. & LAND, C. K. 1989 Transition flight experiments on a swept wing with suction. *Paper* 89-1893. AIAA.

MEITZ, H. L. & FASEL, H. F. 1995 Numerical simulation of boundary-layer flow over suction holes. In *Laminar–Turbulent Transition* (ed. R. Kobayashi), *Proceedings of the IUTAM Symposium*, Sendai, Japan, 1994. Springer.

MESSING, R. 2004 Direkte numerische Simulationen zur diskreten Absaugung in einer dreidimensionalen Grenzschichtströmung. PhD thesis, Universität Stuttgart. Shaker, Aachen, Germany.

MESSING, R., KLOKER, M. J. & WAGNER, S. 1998 Direct numerical simulation of suction through discrete holes in a three-dimensional boundary layer. In *New Results in Numerical and Experimental Fluid Dynamics* (ed. W. Nitsche & R. Hilbig), *STAB/DGLR Symposium*, Berlin, Notes on Numerical Fluid Mechanics, vol. 11. Vieweg.

MÜLLER, W., KLOKER, M. J. & BESTEK, H. 1992 Numerical investigation of the effect of local suction on transition in a boundary layer with adverse pressure gradient. In *DGLR-Bericht 92-06*, *Proceedings of the First European Forum on Laminar Flow Technology*, Hamburg, Germany.

PFENNINGER, W. 1965 Some results from the X-21 A program. Part 1. Flow phenomena at the leading edge of swept wings. In *Recent Developments in Boundary Layer Research*, Part IV, *AGARDograph 97*.

PRALITS, J. O. & HANIFI, A. 2003 Optimization of steady suction for disturbance control on infinite swept wings. *Phys. Fluids* **15** (9), 2756–2772.

PRALITS, J. O., HANIFI, A. & HENNINGSON, D. S. 2002 Adjoint-based optimization of steady suction for disturbance control in incompressible flows. *J. Fluid Mech.* **467**, 129–161.

RENEAUX, J. & BLANCHARD, A. 1992 The design and testing of an airfoil with hybrid laminar flow control. In *DGLR-Bericht 92-06*, *Proceedings of the First European Forum on Laminar Flow Technology*, Hamburg, Germany.

SPALART, P. R. 1993 Numerical study of transition induced by suction devices. In *Proceedings of the International Conference: Near-Wall Turbulent Flows* (ed. R. M. C. So, C. G. Speziale & B. E. Launders), Tempe, AZ, pp. 849–858.

SWARZTRAUBER, P. N. 1977 The methods of cyclic reduction, Fourier analysis and the FACR algorithm for the discrete solution of Poissons equation on a rectangle. *SIAM Rev.* **19** (3), 490–501.

THIBERT, J. J., QUAST, A. & ROBERT, J. P. 1992 The A320 laminar fin programme. In *DGLR-Bericht 92-06*, *Proceedings of the First European Forum on Laminar Flow Technology*, Hamburg, Germany.

WASSERMANN, P. & KLOKER, M. J. 2002 Mechanisms and passive control of crossflow-vortex induced transition in a three-dimensional boundary layer. *J. Fluid Mech.* **456**, 49–84.

WASSERMANN, P. & KLOKER, M. J. 2003 Transition mechanisms induced by travelling crossflow vortices in a three-dimensional boundary layer. *J. Fluid Mech.* **483**, 67–89.

WASSERMANN, P. & KLOKER, M. J. 2005 Transition mechanisms in a three-dimensional boundary-layer flow with pressure-gradient changeover. *J. Fluid Mech.* **530**, 265–293.

WORTMANN, F. X. & WEISE, A. 1970 Der Einfluß der Absaugung durch Poren in der Wand auf die Instabilität laminarer Grenzschichten. *Abschlußbericht* DFG-We 11/37. Institut für Aero- und Gasdynamik, Universität Stuttgart, Germany.